



#### Available online at www.sciencedirect.com

# **ScienceDirect**

Advances in Space Research 73 (2024) 885-917

ADVANCES IN SPACE RESEARCH (a COSPAR publication)

www.elsevier.com/locate/asr

# Composition-property relationships of BP-1 lunar regolith simulant geopolymers for in-situ resource utilization

Thaddeus M. Egnaczyk, William H. Hartt V, Jennifer N. Mills, Norman J. Wagner\*

Center for Neutron Science, Department of Chemical and Biomolecular Engineering, University of Delaware, Newark, DE 19716, United States

Received 8 July 2023; received in revised form 21 October 2023; accepted 20 November 2023 Available online 23 November 2023

#### Abstract

In-situ resource utilization (ISRU) to construct environmental protection and critical infrastructure is required for long-term human habitation on the Moon and Mars. Analogous to terrestrial construction materials formed from aluminosilicates, i.e., geopolymers, construction materials formed from lunar aluminosilicate regolith are a promising method to create lunar landing pads and habitats. Building on a previous lateral study across multiple regolith simulants, the effects of composition on one specific regolith simulant, Black Point 1 (BP-1), are investigated with the goal of developing relationships between composition and properties. The effects of overall geopolymer composition, activating solution silica and sodium content, and activating solution water content on seven-day compressive strength, strain to fail, and secant modulus are investigated. Decreasing water content has a positive effect on compressive strength and secant modulus of geopolymers formed at ambient-earth conditions, reaching maximum compressive strength at 75 wt% BP-1. Above a compositional limit of  $Si/H_2O = 0.6$ , differences in Si and Al coordination result in variations in compressive strength with the elemental composition of the geopolymer. At high solids in formulation, the observed trend in compressive strength is nonmonotonic with varying silicon and aluminum content, emphasizing the need for a mechanistic understanding of the relationship between composition and structure for optimization of geopolymer material properties. This study provides a robust set of data for a widely available lunar regolith simulant that can guide further development of processing strategies for lunar ISRU.

© 2023 COSPAR. Published by Elsevier B.V. This is an open access article under the CC BY license (http://creativecommons.org/licenses/by/4.0/).

Keywords: In-situ resource utilization; Regolith simulants; Geopolymers; Lunar construction

#### 1. Introduction

The construction of permanent structures on the lunar surface is a challenging engineering problem that must be solved in the coming decades (Smith et al., 2020, Anand et al., 2012, Crawford, 2015, Sanders and Larson, 2012). Planned NASA Artemis missions include construction of the Artemis Base Camp at the South Pole of the Moon after Artemis III, requiring a variety of infrastructure including radiation shielding, landing pads, roads, and storage facilities (Creech et al., 2022, Warner, 2020). Fur-

thermore, traditional terrestrial methods of construction are generally not feasible on the lunar surface primarily due to lunar regolith composition, payload limitations, cost, and the harsh environment of the lunar surface (Mills et al., 2022b, Jones, 2018). Thus, lunar infrastructure will necessarily require extensive in-situ resource utilization (ISRU) as well as advances in manufacturing. Steps toward this are rapidly accelerating: In December of 2022, NASA awarded a contract to the Texas based company ICON to develop space-based construction systems, 3D printing lunar regolith into critical lunar infrastructure, reinforcing the need for the rational formulation of suitable lunar construction materials (Frazier, 2022).

E-mail address: wagnernj@udel.edu (N.J. Wagner).

<sup>\*</sup> Corresponding author.

Regolith rich in aluminosilicate (Als) is the primary material available for ISRU-based construction on the lunar surface, comprised of unconsolidated rock and debris material several meters thick (McKay et al., 1991). Regolith is continuously formed from newly exposed lunar bedrock through meteoroid impacts and bombardment of the lunar surface by charged particles (McKay et al., 1991, Papike et al., 1982). A limited amount of lunar regolith is available for study, necessitating the use of lunar regolith simulant materials developed from terrestrial sources for lunar exploration research and development, including ISRU construction solutions (McKay et al., 1993, Ray et al., 2010, Stoeser et al., 2010).

Geopolymer construction materials obtained from natural Als clays are a well-studied class of Als materials currently used for terrestrial construction, and similar chemical activation has been proposed for lunar regolith (Alexiadis et al., 2017, Zhou et al., 2020, Davis et al., 2017, Montes et al., 2015, Mills et al., 2022b, Collins et al., 2022). Formed from the reaction between an aluminosilicate source and an alkaline activating solution, geopolymers are studied as sustainable alternatives to Ordinary Portland Cement (OPC) for construction applications (Davidovits, 2020, Duxson et al., 2007b, Duxson et al., 2006). In this study, and in agreement with the wider geopolymer literature, the term "geopolymer" is used to describe the bulk material formed from the reaction between solid aluminosilicate regolith and liquid alkaline activating solution. The term "binder" describes the gel phase that links aluminosilicate particles together to form strength in the overall geopolymer material (Davidovits, 2020). Geopolymers have been successfully formed from a variety of terrestrial aluminosilicate sources ranging from high purity calcined clays, e.g., metakaolin, to industrial waste products, e.g., granulated blast furnace slag and fly ash (Davidovits, 2020). Large-scale terrestrial geopolymer construction projects include a commercial airport runway (Glasby et al., 2015) and pre-cast structural concrete (Chua, 2013) among others. Critical for lunar applications, geopolymer structure is formed via a net water-neutral reaction (Davidovits, 2020), while cement consumes a water mass of approximately 20 % to 30 % of the cement mass in formulation (Hewlett and Liska, 2019). Such Als materials often display comparable compressive strength (CS), greater resistance to acid attack, and improved thermal properties compared to OPC (Davidovits, 2020).

Numerous studies report formulation and characterization of geopolymer materials formed from lunar regolith simulants for various proposed applications. The lunar regolith simulant Johnson Space Center (JSC-1A) was successfully activated to form a geopolymer, with subsequent studies investigating the effect of particle size, activating solution molarity, and curing conditions on compressive strength (Alexiadis et al., 2017, Davis et al., 2017). Blocks of JSC-1A geopolymer have also been successfully tested as radiation shielding under simulated lunar conditions (Montes et al., 2015). Additional lunar regolith simulant

geopolymers have been synthesized from a variety of source materials with subsequent characterization (Zhou et al., 2020, Collins et al., 2022, Wang et al., 2017). The ultimate goal of additive manufacturing (AM) regolith structures requires additional material processing requirements, as has been analogously developed for AM of traditional cementitious materials (Roussel, 2018). In efforts to formulate a lunar regolith geopolymer with required workability for AM while using chemical admixtures readily available on the moon, urea was investigated as a potential superplasticizer for geopolymers formed from the DNA-1 simulant (Pilehvar et al., 2020).

Despite the rapidly growing body of work forming and characterizing lunar simulant geopolymers, it is often difficult to compare material property results due a lack of standardized geopolymer mixing and curing protocols. A recent study by Mills et al. created a standardized framework to compare geopolymers formed from various lunar and Martian regolith simulants (Mills et al., 2022b). Geopolymers formed from three lunar regolith simulants including Black Point 1 (BP-1), JSC-1A, Lunar Highlands 1 (LHS-1) and one Martian regolith simulant, the Mars Global Simulant (MGS-1C), were tested for CS under different environmental exposure conditions: ambient, vacsub-freezing, and high temperatures. uum, geopolymers cured at elevated temperatures developed CS sufficient for potential use as a vertical takeoff/vertical landing (VTVL) pad. The results of the study by Mills et al. indicate that the variability of chemical composition and processing conditions greatly affect geopolymer compressive strength and optimization of lunar geopolymer mix design is needed before implementation. Specifically, there is a critical need to understand how the composition of lunar regolith geopolymers affects their strength and chemical structure under earth ambient conditions. Additionally, analysis of Apollo regolith determined that regolith chemical composition varies continuously across the lunar surface, with the mare basins containing largely low-titanium basaltic regolith and highlands regolith containing relatively lower levels of magnesium and iron, reinforcing the need to understand how chemical composition affects material properties (Papike et al., 1982, Crawford, 2015). This study aims to address the need to optimize activation and processing of lunar Als to achieve optimal material properties by investigating how the composition of an activating solution and a model lunar regolith simulant, BP-1, affects geopolymer properties and thereby, work towards identifying the minimal required terrestrial resources, as guidance for optimal processing strategies for geopolymers formed by ISRU on the Moon and Mars.

# 1.1. Factors affecting geopolymer material properties

Geopolymer CS is influenced by the aluminosilicate source, composition and alkalinity of activating solution (Al Bakri et al., 2012), particle size of the aluminosilicate precursor (Jamkar et al., 2013), solid to liquid mass ratio,

water content (Barbosa et al., 2000, Hardjito et al., 2004a), and curing temperature (Roynaník, 2010), along with other factors. Fly ash geopolymers are well-characterized and of interest in this study due to chemical similarity with the Black Point 1 regolith simulant (Table 1). In fly ash geopolymers, the type and concentration of the alkaline activating solution has a significant effect on CS. Hardjito et al. specifically studied the alkaline activation of fly ash with sodium hydroxide and sodium silicate in varying molar ratios, finding that a higher concentration of sodium hydroxide results in a higher CS (Hardiito et al., 2004a). Palomo et. al and Al Bakri et. al found that a NaOH activator concentration of 12 M resulted in high CS for metakaolin and fly-ash geopolymers respectively (Palomo et al., 1999, Al Bakri et al., 2012). A subsequent study by Al Bakri et. al found that CS trends were non-monotonic with varying silica to sodium ratio in the activating solution (Al Bakri et al., 2012; Abdullah, 2012)It was observed that at a  $Na_2SiO_3/NaOH$  molar ratio of 2 or Si/(Si + Na) elemental molar ratio of 0.22 the fly ash geopolymer CS significantly decreased, contrary to the overall trend in CS with varying silicon content.

Increasing water content in fly ash geopolymer formulation reduces the seven-day CS of the material, but improves the initial workability of the geopolymer mixture, aiding in material handling and processing (Hardjito et al., 2004a, Vitola et al., 2020, Pouhet et al., 2019, Xie and Kayali, 2014). Maximum fly ash geopolymer CS was observed at a H<sub>2</sub>O/solids ratio of 0.17 by Hardjito et. al, and 0.22 by Xie and Kayali. Jamkar et al. investigated the impact of fly ash particle size on seven-day CS, finding that decreasing particle size results in greater CS, greater workability, and more rapid reaction kinetics (Jamkar et al., 2013). A comprehensive model for geopolymer CS does not yet exist given the large number of input parameters governing property development; however, learnings from compositionally similar systems can be applied to lunar regolith simulant geopolymers to accelerate material design. Hence, in the work presented here we systematically vary the activating solution composition and regolith fraction with guidance from a prior study by Mills et al., (2022b). In a lateral study across lunar and Martian simulants as well as a survey of the literature, the CS was observed to increase as the nominal elemental ratios of the geopolymer approach the elemental ratios of Si/Al = 2 and Na/Al = 1, as codified by a pseudo-ternary state diagram (see Fig. 10 in Mills et al., (2022a)).

#### 1.2. Experimental objectives

The primary aim of this study is to understand how changes in composition affect the material properties of geopolymers formed from BP-1 lunar regolith simulant under a standardized curing protocol. The first objective is to measure material property trends in BP-1 lunar regolith simulant geopolymers of varying composition and determine trends for strength development. BP-1 lunar regolith simulant is selected specifically due to its current use by NASA and relatively high CS when cured under ambient and vacuum conditions. The geopolymer composition space is explored by varying water content, silica content, and sodium content following the aforementioned guidance on formulation design from Mills et al., (2022b). The second objective of this work is to empirically connect trends in CS of the BP-1 geopolymers with chemical structure of the geopolymer binder across formulation compositions. Such information is necessary for developing a mechanistic understanding of the nano- to microstructural origins of geopolymer strength. This study represents a necessary step towards the rational engineering of Als construction materials for a broad range of uses including additive manufacturing of geopolymers for terrestrial applications and lunar ISRU applications for geopolymers.

#### 2. Materials and methods

#### 2.1. Materials

# 2.1.1. Black Point 1 lunar regolith simulant

The Black Point 1 (BP-1) lunar regolith simulant is selected as it is well-studied and developed high CS when cured under ambient conditions by Mills et al., (2022b). It is also used as a geotechnical simulant for NASA's Lunabotics competitions, where robots are challenged with

Table 1 Bulk chemistry analysis (wt%) of the Black Point 1 simulant material, compared to a generic class F fly ash. and terrestrial metakaolin composition. LOI = Loss on ignition. Trace elements (<0.5%) including NiO, SrO, Cr<sub>2</sub>O<sub>3</sub> are omitted from this table but may be reported in the sources indicated.

Oxide	<b>BP-1</b> (Stoeser et al., 2010)	Fly ash, Class F (Typical) (Mindess et al., 2003)	Metakaolin
SiO <sub>2</sub>	47.2	>50	55
$TiO_2$	2.3		1.5
$Al_2O_3$	16.7	20–30	40
$FeO_T$	12.1	<20	1.4
MgO	6.5		
CaO	9.2	<5	
Na <sub>2</sub> O	3.5		
$K_2O$	1.1		0.8
MnO	0.21		
$P_2O_5$	0.52		
LOI			1
Total	99.33		99.7

building a berm out of lunar regolith simulant (Heiney, 2020). BP-1 is obtained from the Kennedy Space Center's Swamp Works Group and is sourced from the Black Point basalt flow in the San Francisco Volcanic Field in northern Arizona (Suescun-Florez et al., 2015). An image of BP-1 regolith powder is shown in Fig. 1 and Table 1 provides a bulk chemical analysis of BP-1 along with a common class F fly ash. The particle size distribution of BP-1 fits within the  $\pm$  1 standard deviation range of lunar regolith particle size and is more representative of lunar regolith than other available lunar regolith simulants including JSC-1A (Suescun-Florez et al., 2015). Like high-fidelity simulants, the particle shape of BP-1 is described as rough and angular. BP-1 contains a high content of fine material with anomalous large gravel pieces. BP-1 densifies under compaction at a slightly slower but similar rate to highfidelity simulants (Rahmatian and Metzger, 2010). The average specific gravity (particle density) of BP-1 is slightly lower than JSC-1A and significantly lower than Minnesota lunar simulant 1 (MLS-1) and lunar regolith (Suescun-Florez et al., 2015).

In this study, the BP-1 simulant particle size is standardized using a #200 sieve (75  $\mu m)$  to remove large particles and small stones. The simulant volume-based particle size distribution was measured using a Beckman Coulter LS 13 320 Particle Size Analyzer with dry powder module. Table 2 lists the particle size limits for 10, 50, and 90 % of the cumulative distribution of the simulant.

BP-1 composition is well characterized as a continental basalt with relatively high alkaline content, similar to lunar mare soils with a high plagioclase content (Stoeser et al., 2010). Important for comparison to other aluminosilicate sources, Table 3 provides mole fractions and ratios relevant for geopolymer formation. The molar analysis in Table 3 shows that TiO<sub>2</sub>, MnO, P<sub>2</sub>O<sub>5</sub>, and K<sub>2</sub>O are likely not critical components to consider for the geopolymer reaction due to their relatively low molar ratios.



Fig. 1. Black Point 1 lunar regolith simulant.

Table 2 Particle size distribution analysis by laser diffraction of sieved BP-1 lunar regolith simulant, where 10% of the distribution (by volume) has a particle size (diameter) less than the d10 particle size (etc. for d50, d90).

Sieved BP-1 Particle Size (μm)				
d10	1.5			
d50	22.7			
d90	65.1			

The compositional variation of geopolymers with differing nominal elemental ratios of sodium, silicon, and aluminum can be visualized via a pseudo-ternary state diagram for alkali-activated materials (Mills et al., 2022a). The location of BP-1 on pseudo-ternary state diagram along with other representative lunar simulant materials is shown in Fig. 2. The composition listed in Table 3 indicates that BP-1 contains iron oxides, calcium oxide, and magnesium oxide in addition to the desired aluminum and silicon oxides, which may also play a role in property development (Mills et al., 2022b, Bakharev, 2005, Kaze et al., 2017, Nongnuang et al., 2021, Rickard et al., 2010).

#### 2.1.2. Sodium silicate activating solutions

Sodium silicate activating solutions are created from deionized water (Millipore Milli-Q 18.2 M $\Omega$ ), sodium hydroxide pellets (Fischer Scientific CAS: 1310–73-2), and fumed silica (Cabot CAB-O-SIL EH-5 Hydrophilic Fumed Silica) to have desired water content (wt% H<sub>2</sub>O) and molar ratio of silicon and sodium Si/(Si + Na), written as Si/ $\Sigma$ . Water and sodium hydroxide pellets are mixed in a stainless-steel beaker for thirty minutes with a magnetic stir bar while covered, allowing for full dissolution of the sodium hydroxide and cooling to room temperature after the exothermic dissolution. Fumed silica is then added, and the solution is mixed for at least 24 h before use in geopolymer synthesis. The work is performed at laboratory temperature ( $\sim$ 18  $\pm$  1.5 °C).

The relative silica and sodium content of each activating solution is varied in terms of elemental ratios, ranging from 0.3 to  $0.6\mathrm{Si}/\Sigma$ . Two levels of water content in the activating solution are investigated, 45 and 60 wt% H<sub>2</sub>O. Table 4 below lists the per-gram formulation of each activating solution used in this study. Activation solution pH was measured using an Oakton 700 benchtop pH meter.

Activating solutions with high fumed silica content and low water content required a longer mixing time. Fumed silica was added in successive steps over the course of 48 h to prevent clumping and solidification of the mixture. Extended mixing times are required for activating solution compositions of 0.4 and  $0.5 \text{Si}/\Sigma$  at water content of 45 wt%  $H_2O$ . An activating solution at a composition of  $0.6 \text{Si}/\Sigma$  and 45 wt%  $H_2O$  could not be formed at ambient conditions due to the relatively large amount of fumed silica in formulation, despite attempts to add the fumed silica powder to the pre-mixed water and sodium hydroxide over the course of several days.

Table 3 Molar ratio analysis of Black Point 1 lunar regolith simulant ( $M_{OX} = Moles$  of oxide in each row).

Oxide	BP-1 wt%	Molar Mass (g/mol)	Moles (Oxides)	Oxide Mol %	Moles (Atomic)	Atomic Mol %	SiO2/Mox Ratio
SiO <sub>2</sub>	47.20 %	60	7.87E-03	50.82 %	7.87E-03	44.11 %	1.00
$TiO_2$	2.30 %	79.9	2.88E-04	1.86 %	2.88E-04	1.61 %	27.33
$Al_2O_3$	16.70 %	102	1.64E-03	10.58 %	3.27E-03	18.36 %	2.40
FeOt	12.10 %	71.8	1.69E-03	10.89 %	1.69E-03	9.45 %	4.67
MgO	6.50 %	40.3	1.61E-03	10.42 %	1.61E-03	9.04 %	4.88
CaO	9.20 %	56	1.64E-03	10.61 %	1.64E-03	9.21 %	4.79
Na <sub>2</sub> O	3.50 %	62	5.65E-04	3.65 %	1.13E-03	6.33 %	6.97
$K_2O$	1.10 %	94.2	1.17E-04	0.75 %	2.34E-04	1.31 %	33.68
MnO	0.21 %	70.9	2.96E-05	0.19 %	2.96E-05	0.17 %	265.59
$P_2O_5$	0.52 %	142	3.66E-05	0.24 %	7.32E-05	0.41 %	107.41
Total	0.9933		1.55E-02	100.00 %	1.78E-02	100.00 %	

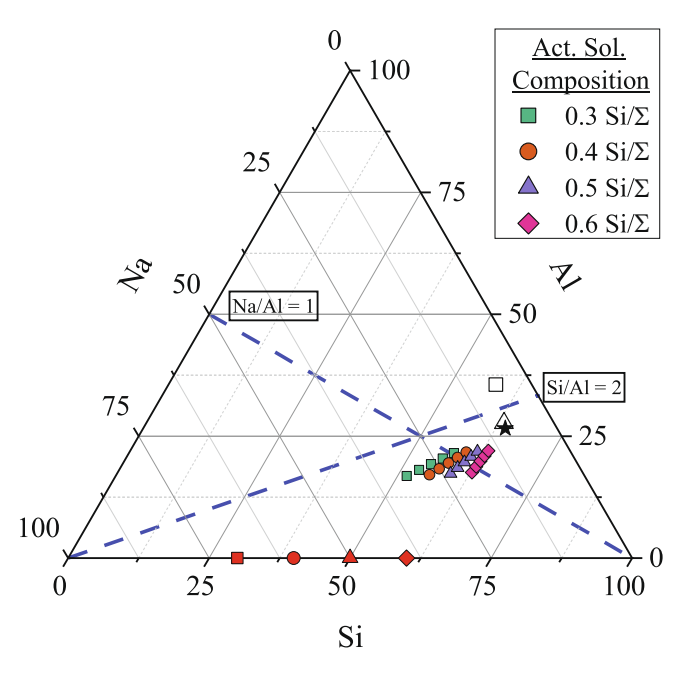


Fig. 2. Pseudo-ternary state diagram. Lunar regolith simulants: BP-1 (black star), JSC-1A (open triangle), LHS-1 (open square). Sodium silicate activating solutions (red symbols on Si axis). BP-1 geopolymers formed from the following activating solutions:  $0.3\text{Si}/\Sigma$  (green squares),  $0.4\text{Si}/\Sigma$  (orange circles),  $0.5\text{Si}/\Sigma$  (purple triangles),  $0.6\text{Si}/\Sigma$  (pink diamonds). Dashed lines identify theoretically optimal Si/Al and Na/Al ratios.

#### 2.2. Geopolymer formation

#### 2.2.1. Mixing protocol

BP-1 geopolymers were created from BP-1 lunar regolith simulant and sodium silicate activating solutions. Simulant and activating solution were measured into (150 mL) plastic mixing cups and then mixed by hand with a stainless-steel spatula for a period of five minutes. Cubes created from the  $0.3\text{Si}/\Sigma$  (60 H<sub>2</sub>O) activation solution were mixed for  $\sim 2$  min and immediately packed in the molds due to rapid reaction. After mixing, the geopolymer precursor mixture was transferred into 1 cm³ silicone rubber cube molds open on one surface. Eight cubes were created for each geopolymer composition. The average density of a given geopolymer precursor paste was recorded immediately after mixing by measuring the mass of four cubes in the silicone mold and dividing by the mold volume.

#### 2.2.2. BP-1 geopolymer formulation

Geopolymer compositions tested in this study were selected to cover a range of (1) simulant to activating solution mass ratios, (2) water content, and (3) relative silica to sodium content in the activating solution which are practically feasible for geopolymer preparation. Chemical composition (nominal Si/Al/Na ratio) of the geopolymers is controlled via the sodium silicate activating solution and weight percent of BP-1 in formulation. Geopolymer com-

Table 4 Composition of sodium silicate activating solutions on a per-gram basis.  $Si/\Sigma$  represents Si/(Si+Na) and  $(\cdot H_2O)$  represents the weight percent of water in the activating solution.

<b>Activating Solution</b>	Mass H <sub>2</sub> O	Mass NaOH	Mass SiO <sub>2</sub>	Elemental Si/Σ	pН	NaOH Molarity
0.3Si/Σ (60 H <sub>2</sub> O)	0.60	0.24	0.16	0.30	13.9	10.1
$0.4 \text{Si}/\Sigma \ (60 \text{ H}_2 \text{O})$	0.60	0.20	0.20	0.40	13.4	8.3
$0.5 \text{Si/}\Sigma \ (60 \text{ H}_2\text{O})$	0.60	0.16	0.24	0.50	12.7	6.7
$0.6\text{Si/}\Sigma \ (60 \text{ H}_2\text{O})$	0.60	0.12	0.28	0.60	11.7	5.1
$0.4\text{Si}/\Sigma (45 \text{ H}_2\text{O})$	0.45	0.27	0.28	0.40	13.8	15.3
$0.5 \text{Si}/\Sigma \text{ (45 H}_2\text{O)}$	0.45	0.22	0.33	0.50	13.3	12.2

position is varied from 55 to 75 wt% BP-1 simulant with the activating solution as the remaining balance. Table A2 in the Appendix lists all BP-1 geopolymer compositions created for this study on a per gram basis. In this work the term "composition series" refers to the series of five BP-1 geopolymer compositions made from a given sodium silicate activating solution, with varying wt% BP-1 in formulation from 55 to 75 wt% in increments of five percent.

A pseudo-ternary state diagram for alkali-activated materials, Fig. 2, is used as an organizing framework for BP-1 geopolymer compositions (Mills et al., 2022a). The ternary diagram relates the nominal elemental ratios of silicon, aluminum, and sodium (Si/Al/Na) in each geopolymer sample. Fig. 2 is a "pseudo" ternary diagram as water, along with other BP-1 constituent minerals that may impact binder strength like calcium, are not included on this plot and compositions are nominal starting compositions, not solution compositions in the dissolved phase or final compositions of the geopolymer formed. BP-1 regolith simulant composition and other representative lunar regolith simulant compositions are also plotted in Fig. 2. The nominal Si/Al/Na ratio of the activating solutions created for this study are also represented. All geopolymer compositions are described as nominal due to the likely incomplete dissolution of BP-1 as the aluminosilicate source (Fernández-Jimenez et al., 2006). Dashed blue lines indicate nominal elemental ratios of Si/Al = 2 and Na/ Al = 1 as theoretical optimums suggested from the geopolymer literature (Mills et al., 2022a).

# 2.2.3. Curing protocol

Geopolymer cubes were cured in 1 cm<sup>3</sup> silicone molds, open to the atmosphere on the top, for seven days at ambient laboratory conditions. The ambient laboratory temperature was  $18 \pm 1.5$  °C during all experiments. Weight loss due to any evaporation was gravimetrically monitored.

#### 2.3. Geopolymer characterization

#### 2.3.1. Compressive strength testing

Protocols developed in prior work were followed here (Mills et al., 2022b). Compression testing was performed using an Instron 5965 dual column table frame with Blue-Hill operating software. The load cell was an Instron model 2580–108 with a force capacity of 5 kN. Cubes were compressed between two platens using a modified ASTM C109 compression protocol, *Compression testing of hydraulic cement mortars* (ASTM International, 2020). The protocol was modified for the reduced cube size (1 cm<sup>3</sup> compared to 2 in.<sup>3</sup> in the protocol) and cure time (seven-day cure time versus the 28-day cure time required for cementitious materials). Compression was programmed at a rate of 1 mm/min.

The cube face normal to the top platen was manually smoothed with sandpaper to create a flat surface for compression testing. Cube mass and dimensions were recorded for calculation of cured cube density and CS. Geopolymer CS was assessed at seven days to compare to relevant geopolymer literature and due to studies showing that geopolymer CS increases most rapidly in the initial 48 h after synthesis and minimally between one and two weeks (Mills et al., 2022b, Hardjito et al., 2004a, Palomo et al., 2004, Davidovits, 2020).

Compression testing was performed for 6–8 replicate cubes of each composition. The force displacement curve for each cube was transformed to engineering stress  $(\sigma, \text{Eq.}(1))$  and engineering strain  $(\epsilon, \text{Eq.}(2))$ , where F and  $\Delta h$  are the measured force and displacement, and h and A are height and contact surface area of each individual cube.

$$\sigma = F/A \tag{1}$$

$$\varepsilon = \Delta h/h \tag{2}$$

Individual stress—strain curves were fit to a cubic spline utilizing the algorithm scipy.interpolate. UnivariateSpline in Python, corrected for any zero offset in initial position and averaged. The procedure is illustrated in Fig. 3, where the six individual tests are averaged to form the curve and uncertainty bound plotted in Fig. 3B. The band in Fig. 3B represents one standard deviation at each strain.

The CS was determined by one of two methods depending on the behavior of the sample. For samples exhibiting distinct material failure at a maximum tensile force, the CS was identified as the maximum stress, as shown in Fig. 4A, along with the associated strain to fail. Red X's on Fig. 4A indicate the maximum stress on the averaged stress-strain curve as well as the maximum stress of the averaged stress  $\pm$  1 standard deviation curves, allowing for an estimation of uncertainty in both the maximum stress (vertical) and strain to fail (horizontal). For samples that displayed a more plastic failure without a distinct maximum, the transition to plastic failure is identified as the CS as shown in Fig. 4B. Two lines were extended in linear regions of the curve, and the stress value at the intersection of the two linear regimes is assigned as the CS along with the strain value as the strain to fail. The standard deviation was determined by performing the same procedure for the bounding curves as shown.

The secant modulus, a common measure of the modulus of elasticity or Young's modulus in concrete materials, was determined by utilizing the equation for the secant modulus, or chord modulus of elasticity, in ASTM C469, *Static Modulus of Elasticity and Poisson's Ratio of Concrete in Compression*, (Eq. (3)), where E is the secant modulus,  $\sigma_2$  is 40 % of the CS,  $\varepsilon_1$  a strain of 0.000050,  $\varepsilon_2$  is the corresponding strain to  $\sigma_2$ , and  $\sigma_1$  is the corresponding stress to  $\varepsilon_1$ (ASTM International, 2022). The value of  $\sigma_1$  was interpolated from the data.

$$E = (\sigma_2 - \sigma_1)/(\varepsilon_2 - \varepsilon_1) \tag{3}$$

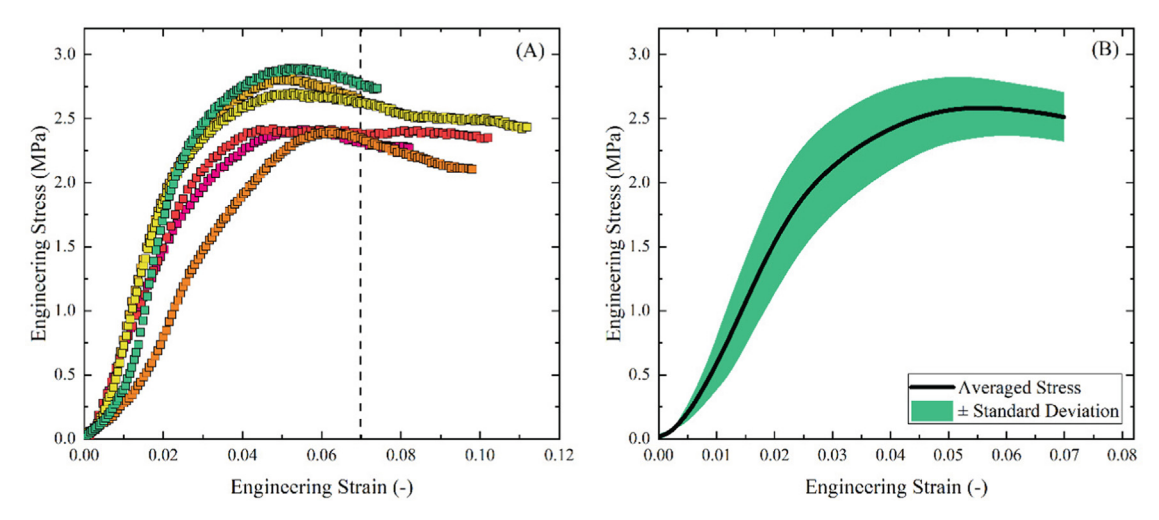


Fig. 3. (A) Engineering stress–strain curves for 6 samples of BP-1 geopolymer created with 70 wt% BP-1, an activating solution of nominal molar ratio  $0.3Si/\Sigma$ , and an activating solution of 60 wt% water. Values are considered up to the first end of a sample (dashed line). (B) Averaged engineering stress–strain curve of individual stress–strain curves in Fig. 3A up to the first endpoint of an experiment. Green band represents  $\pm 1$  standard deviation.

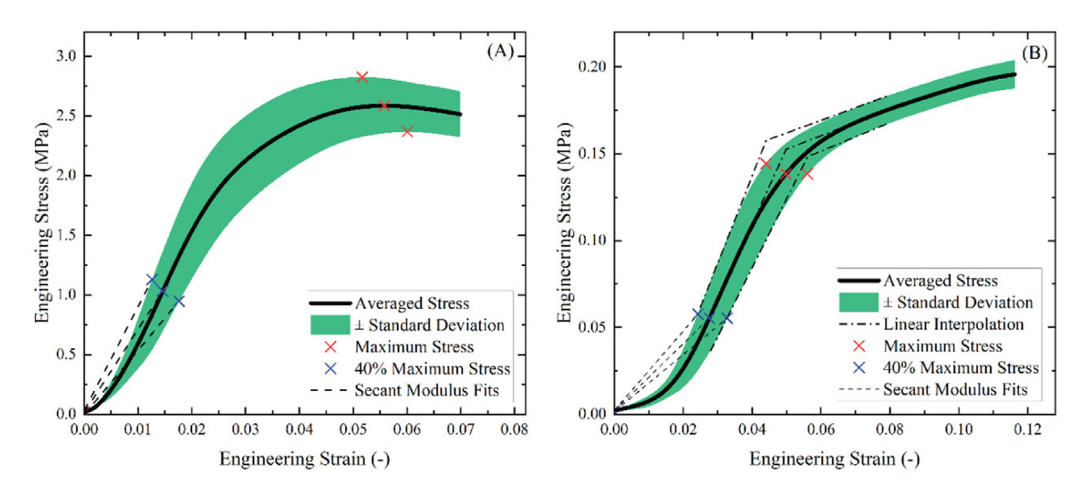


Fig. 4. (A) Standard method for calculation of compressive strength utilizing the maximum value of the averaged stress curve, as well as the maximum of the average stress  $\pm$  1 standard deviation curves. A visual representation of the secant modulus calculation is shown. Averaged curve shown from Fig. 3B. (B) Alternative method for calculation for compressive strength when there is no maximum value in the averaged stress curve. The interception of two linear interpolations is vertically dropped down to the stress curve. A visual representation of the secant modulus calculation is shown. The represented curve is a BP-1 geopolymer with a BP-1 wt% of 55 %, a nominal molar ratio is  $0.3Si/\Sigma$  in the activating solution, and an activating solution of 60 wt% water.

# 2.3.2. Mass loss measurements

Mass loss to the environment during ambient curing was calculated for each composition as the percent change in mass from the initial geopolymer paste after mixing to the final cured sample mass at seven days. Initial water content data is known from the activating solution water content and density of geopolymer precursor mixture in each mold. Inherent water content of the BP-1 simulant is 3.68  $\pm$  0.01 wt%, determined via thermogravimetric analysis (TGA). Three samples of sieved BP-1 were measured in a Discovery TGA using a ramp protocol of 20 °C per minute to a final temperature of 700 °C, followed by a 10-minute isothermal hold. Water content was assessed as the average mass loss of the three trials after the isothermal hold. Average initial geopolymer cube mass after mixing was deter-

mined by dividing the mass of four cubes in silicone molds by four. The final mass and dimensions of each individual cube was measured immediately before CS testing.

# 2.3.3. Nuclear magnetic resonance spectroscopy (NMR)

Solid-state <sup>27</sup>Al and <sup>29</sup>Si magic angle spinning (MAS) NMR spectra were obtained using a 4.0 mm HX probe (AVIII 500 SSNMR, Bruker, Billerica, MA). The BP-1 geopolymer samples studied with NMR were created seven days in advance of the NMR measurements for chemical similarity with samples tested for CS, using the same preparation and curing protocols. Cubes were pulverized with a mortar and pestle to create a powder/paste for loading into the NMR rotor. <sup>27</sup>Al MAS NMR spectra were acquired at 12 kHz with a single pulse of 1 µs and a pulse delay of 1 s

(512 scans each). <sup>29</sup>Si CP/MAS NMR spectra were acquired at 12 kHz with 7 ms CP contact time and a pulse delay of 3 s. Cross-polarization was necessary to obtain a suitable signal in the silicon spectra, as has been used previously in amorphous aluminosilicate materials (Mills et al., 2022b, Doucet et al., 2001, Houston et al., 2008). A 4 mm reduced volume rotor with a spacer was used for dense samples. A sample mass of  $\sim 0.08$  g provided well-resolved signal to noise ratio.

Following established procedures (Engelhardt and Michel, 1987, Giuli et al., 1999, Valcke et al., 2015, Lee and Stebbins, 1999), <sup>29</sup>Si NMR spectra were deconvoluted into gaussian peaks representing the expected Q<sup>n</sup> (mAl) sites using a Levenberg-Marquardt algorithm. Table 5 presents the expected ranges of chemical shifts for Q<sup>n</sup>(mAl) species in silicate and aluminosilicate samples used as bounds for peak deconvolution (Davidovits, 2020, Engelhardt and Michel, 1987). An example plot showing deconvoluted peaks for a BP-1 geopolymer sample is presented in Fig. 5. The third column in Table 5 lists the peak assignments and relative amounts for this specific sample.

#### 3. Results

#### 3.1. Geopolymer precursor mixture

As the relative amount of BP-1 increases within a given composition series, the geopolymer precursor mixture varied from a dark brown liquid which readily flows at 55 wt% to a wet clumped solid at 75 wt%. Compositions with wt% BP-1 between the two extremes of 55 and 75 wt% followed this trend where at 60 and 65 wt% BP-1 the mixture progressively increased in viscosity but still flowed under gravity. The 70 wt% samples mixed easily into a uniform paste but did not flow under gravity. Compositions at low BP-1 wt% (55, 60, 65 wt%) were easily poured into the 1 cm³ cube molds. The 70 and 75 wt% BP-1 compositions required packing with a metal spatula. Tamping molded cubes helped to release air bubbles trapped in the mold from the pouring and packing processes.

Rapid reaction of the geopolymer mixture to form a solid mass occurred during mixing of the  $0.3\text{Si}/\Sigma$  (60

Table 5
Ranges of <sup>29</sup>Si chemical shifts for Q<sup>n</sup>(mAl) components in silicate and aluminosilicate materials relevant to geopolymer systems in this study (Davidovits, 2020, Engelhardt and Michel, 1987).

Q <sup>n</sup> (mAl)	-δ (ppm)	Relative Amount (%) (Fig. 5)
$Q^0(0A1)$	66–73	N/A
$Q^1(0A1)$	76–83	N/A
$Q^1(1A1)$	75	N/A
$Q^2(2A1)$	80	3.6
$Q^4(0Al)$	103-120	7.7
$Q^4(1Al)$	97-105	18
$Q^4(2A1)$	92-99	18
$Q^4(3A1)$	88–94	18
$Q^4(4Al)$	83–87	34

 $\rm H_2O)$  and 0.3Si/Σ (45  $\rm H_2O$ ) compositions, indicated by noticeable heat release through the plastic mixing cup. No geopolymer cubes could be formed from the 0.3Si/Σ (45  $\rm H_2O$ ) activating solution as the BP-1 powder and activating solution formed a hard solid immediately during mixing. At higher water content, 0.3Si/Σ (60  $\rm H_2O$ ), activating solution and BP-1 powder could be mixed but would harden rapidly and could not be mixed for the full fiveminute period.

#### 3.2. Morphology of geopolymer cubes

#### 3.2.1. Morphology before compression

Significant differences in appearance were evident after seven days of ambient curing for geopolymers with varying silica content and BP-1 wt% in formulation. Images of three composition series of BP-1 geopolymer cubes are shown in Fig. 6 (A-C). Visible shrinkage was present in cubes formed at 55 and 60 wt% BP-1 from activating solutions with 60 wt% H<sub>2</sub>O likely due to the relatively high water content of the geopolymer precursor mixture. Increasing BP-1 wt% from 55 to 75 wt% resulted in decreased shrinkage of the cube, with no visible shrinkage present in the 70 and 75 wt% formulations. The 55 wt% BP-1 cubes were soft to the touch and required careful handling during removal from the cube mold to prevent warping of the cube faces before compression. Cubes formed at 55 and 60 wt% BP-1 and higher water content exhibited a thin, clear film on the surface of the cubes exposed to the atmosphere. This clear film is likely composed of silica species from excess activating solution transported to the surface of the cube by water during evaporation.

Geopolymers cubes of 65 to 75 wt% BP-1 were easily removed from the cube mold and sanded. A chalky white residue was commonly found on the surface of cubes formed at 70 and 75 wt% BP-1. Visually similar to efflorescence in cement formation, the white residue on the geopolymer surface are likely salts deposited by water that had migrated to the surfaces of the cube and subsequently evaporated during the curing process (Barbosa et al., 2000, He et al., 2016). Small pockets of air are present in most cubes presented in Figs. 6-9, likely due to air trapped in the cube mold during the cube casting process. A minimum of six cubes were tested for CS for each composition, minimizing the potential impact of air bubbles on the average CS of a given BP-1 geopolymer composition.

# 3.2.2. Fracture behavior of cubes after compression

Fracture behavior differed greatly for geopolymers within a given composition series, changing from a crumbling response as shown in Fig. 7A2 at 55 wt% BP-1 to a vertical brittle fracture at 75 wt% BP-1 as shown by Fig. 8C2 for geopolymers formed from the 0.5Si/ $\Sigma$  (60 H<sub>2</sub>O) activating solution. Similar trends in fracture behavior with BP-1 wt% were observed at lower water content, shown by Fig. 8 for the 0.5Si/ $\Sigma$  (45 H<sub>2</sub>O) composition series.

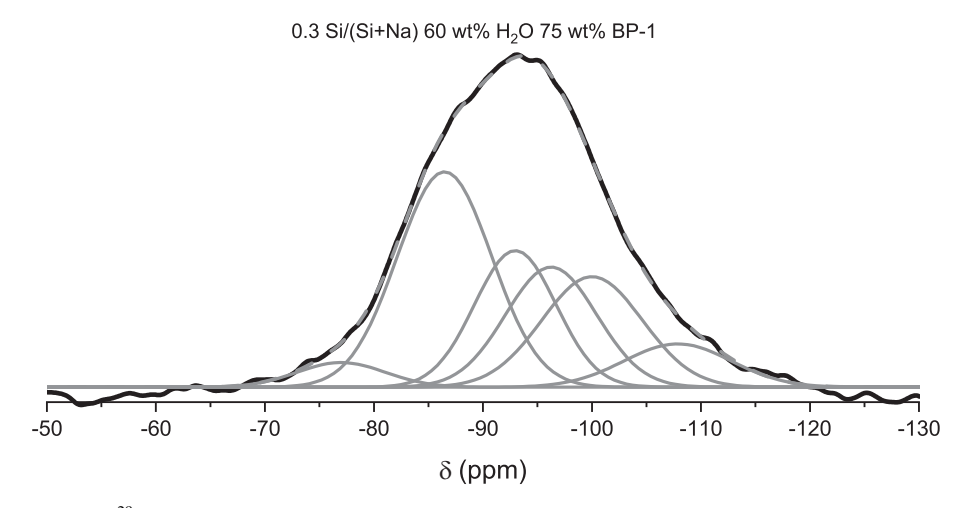
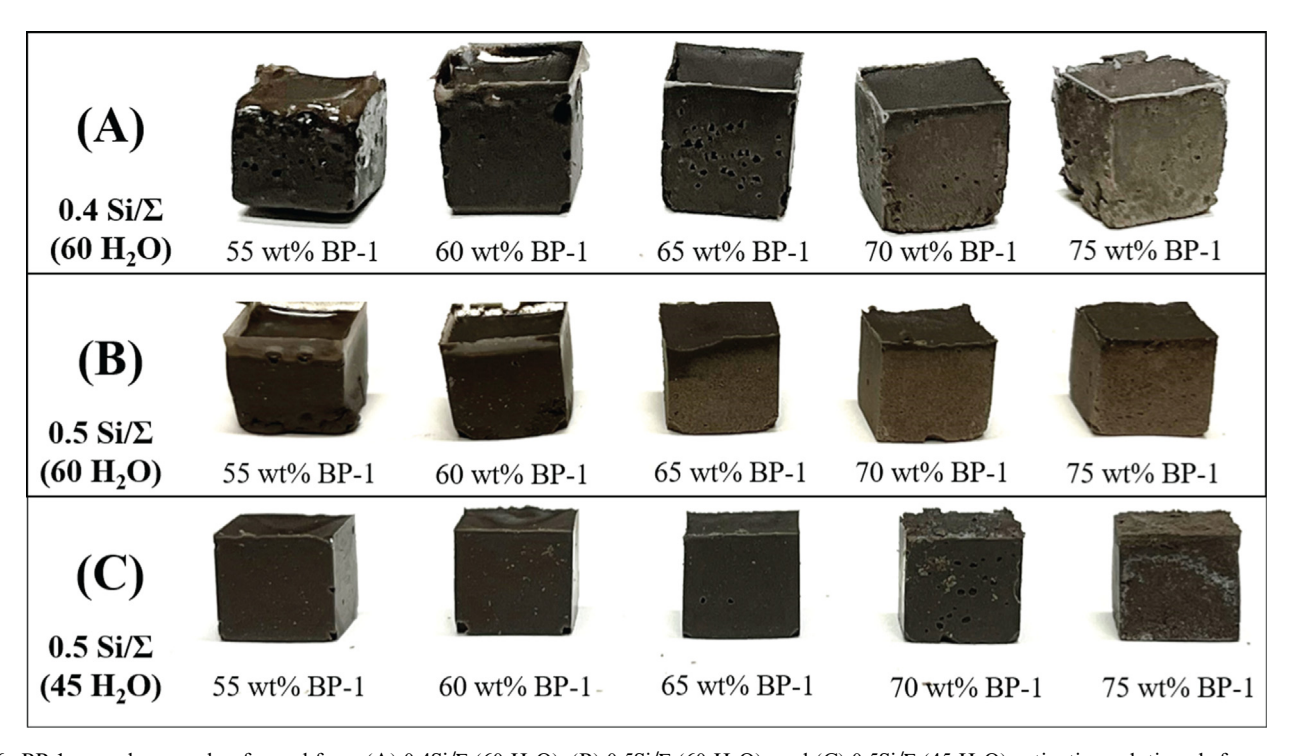


Fig. 5. Example deconvolution of  $^{29}$ Si MAS NMR spectra of seven-day cured 75 wt% BP-1 0.3Si/ $\Sigma$  (60  $H_2$ O) geopolymer into five gaussian peaks representing chemical shifts listed in Table 5. Solid black line represents the experimental  $^{29}$ Si spectra and gray lines show the fitted curves at each assigned peak location.



 $Fig.~6.~BP-1~geopolymer~cubes~formed~from~(A)~0.4Si/\Sigma~(60~H_2O),~(B)~0.5Si/\Sigma~(60~H_2O),~and~(C)~0.5Si/\Sigma~(45~H_2O)~activating~solutions~before~sanding.$ 

Fracture behavior at 55 wt% BP-1 varied significantly based on the nominal silica to sodium ratio in formulation, shown in Fig. 9. The  $0.3\text{Si}/\Sigma$  (60 H<sub>2</sub>O) composition displayed more brittle fracture behavior (Fig. 9A) while all compositions at higher nominal ratios of Si/ $\Sigma$  flattened or crumbled plastically shown in Fig. 9B and 9C. The rapid hardening of the  $0.3\text{Si}/\Sigma$  (60 H<sub>2</sub>O) composition mentioned previously in Section 3.1.2 is likely connected to this difference in fracture behavior. Contrastingly, brittle fracture behavior was observed for all samples formed at 75 wt% BP-1 regardless of the relative silica to sodium nominal ratio within the material.

### 3.3. Measured material properties

3.3.1. Effect of BP-1 wt% on seven-day compressive strength The seven-day CS for all geopolymer compositions are summarized in Fig. 10. Individual stress–strain curves are located in Appendix Figs. A1-10. All measured material property values are provided in Table A3 in the Appendix. The maximum seven-day CS of 5.3 MPa was observed at a formulation of 75 wt% BP-1 0.3Si/Σ (60 H<sub>2</sub>O). Geopolymers formed at 55 and 60 wt% BP-1 from 60 wt% H<sub>2</sub>O activating solutions and 55 wt% BP-1 from the 45 wt% water activating solutions showed almost negligible (<1 MPa)

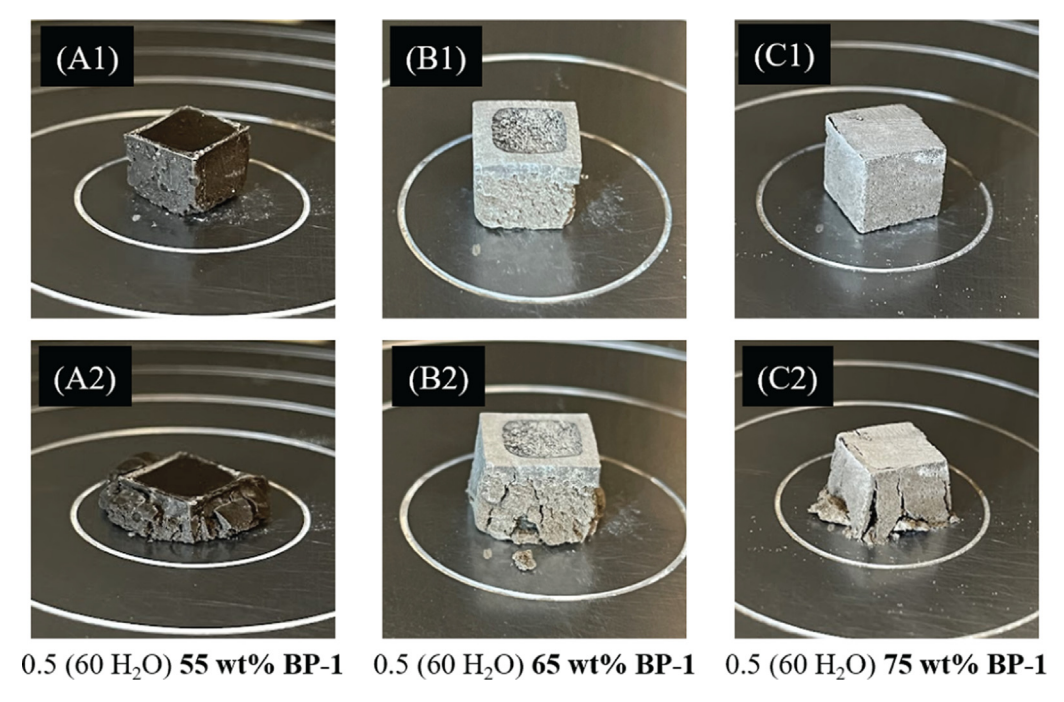


Fig. 7. Fracture behavior of BP-1 geopolymer cubes formed from the 0.5Si/Σ (60 H<sub>2</sub>O) activating solution at representative compositions of (A) 55, (B) 65, and (C) 75 wt% BP-1 in formulation. Cubes shown have been sanded to create a uniform planar surface for compression.

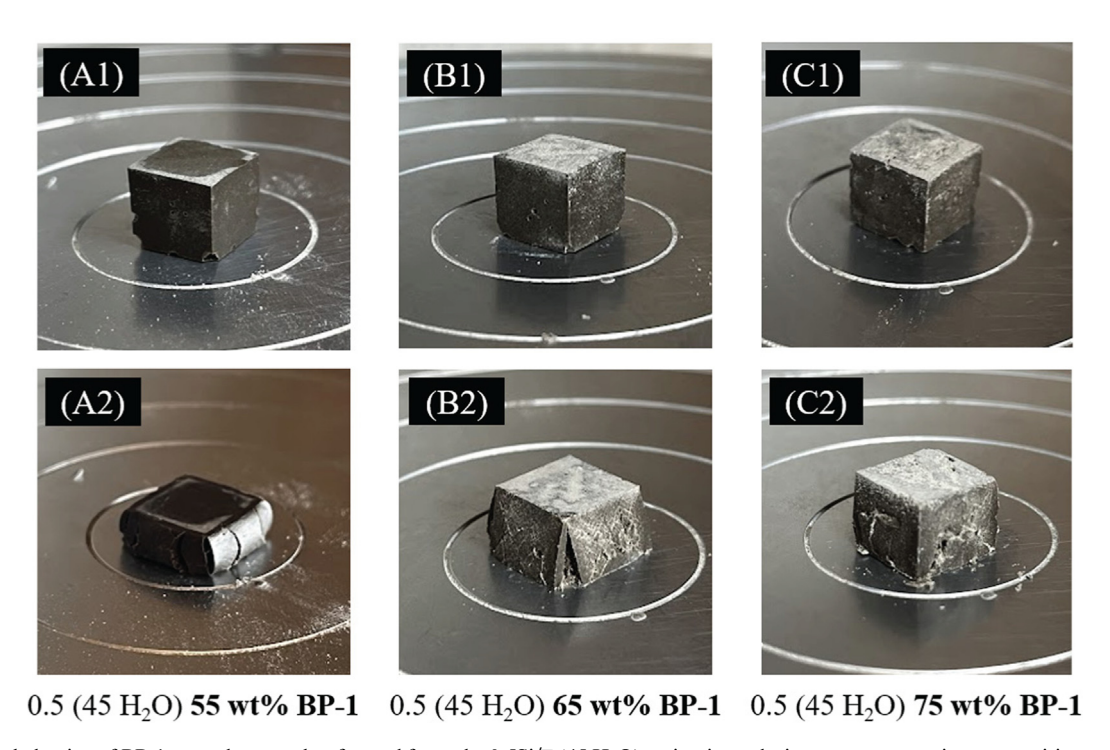


Fig. 8. Fracture behavior of BP-1 geopolymer cubes formed from the 0.5Si/Σ (45 H<sub>2</sub>O) activating solution at representative compositions of (A) 55, (B) 65, and (C) 75 wt% BP-1 in formulation. Cubes shown have been sanded to create a uniform planar surface for compression.

CS across all activating solution compositions. Geopolymers at 55 and 60 wt% BP-1 in the  $0.4\text{Si}/\Sigma$  (45 H<sub>2</sub>O) composition series did not form a measurable CS at seven days.

CS results are compared for the 60 wt% H<sub>2</sub>O activator solutions with varying Si ratios and BP-1 wt% in Fig. 10A. CS increases monotonically with BP-1 wt%

within each activator composition series, obtaining a maximum value at 75 wt% of BP-1. Comparing between composition series at each BP-1 wt% in Fig. 10A, the  $0.4\text{Si}/\Sigma$  (60 H<sub>2</sub>O) composition series show reduced CS for formulations greater than 60 wt% BP-1. Potential origins of the unexpected decreased CS for the  $0.4\text{Si}/\Sigma$  (60 H<sub>2</sub>O) compo-

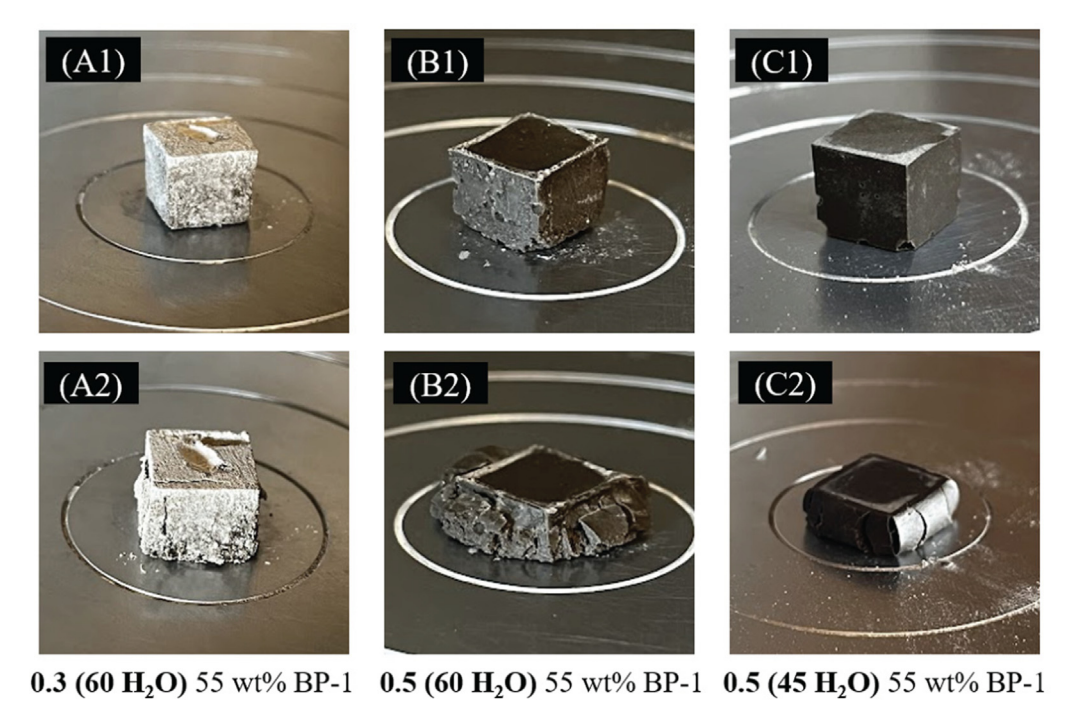


Fig. 9. Fracture behavior of BP-1geopolymer cubes formed from the (A)  $0.3\text{Si}/\Sigma$  (60 H2O), (B)  $0.5\text{Si}/\Sigma$  (60 H2O), and (C)  $0.5\text{Si}/\Sigma$  (45 H2O) activating solution at a constant composition of 55 wt% BP-1.

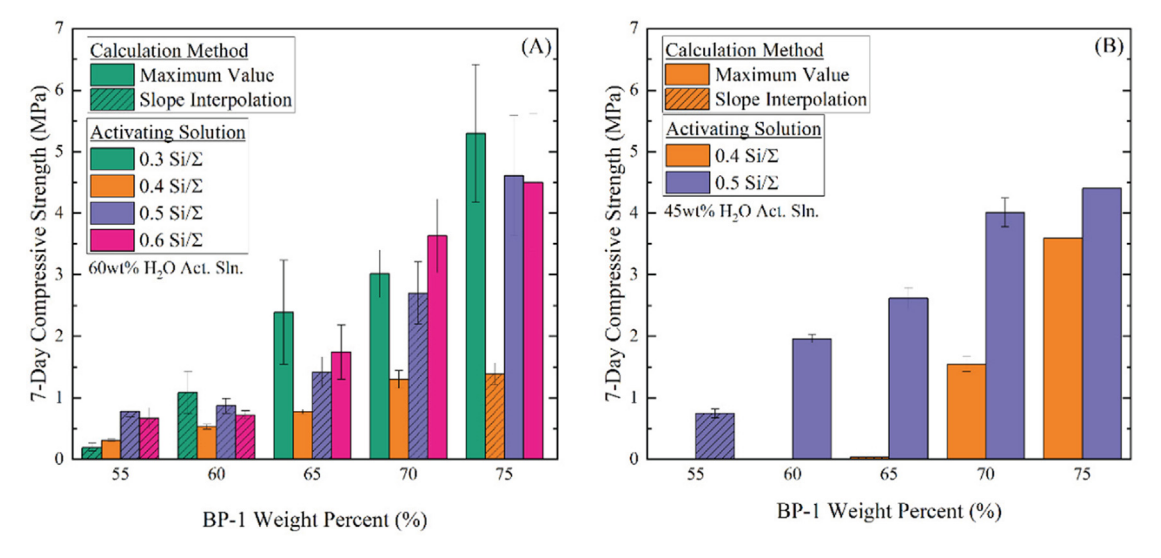


Fig. 10. (A) Seven-day compressive strength of BP-1 geopolymers of varying weight percent (55, 60, 65, 70, and 75) and varying activating solution Si/ $\Sigma$  molar ratios (0.3, 0.4, 0.5, and 0.6) at an activating solution of 60 wt% water cured under ambient conditions. Error bars represent one standard deviation of the replicates. Bar shading represents compressive strength calculation method. Three trials were performed for  $0.4\text{Si}/\Sigma$  and two trials were performed for  $0.3\text{Si}/\Sigma$  and  $0.5\text{Si}/\Sigma$ . (B) Seven-day compressive strength of BP-1 geopolymers of varying weight percent (55, 60, 65, 70, and 75) at Si/ $\Sigma$  molar ratios of 0.4 and 0.5 with an activating solution of 45 wt% water cured under ambient conditions. Geopolymers made with 55 and 60 wt% BP-1 at  $0.4\text{Si}/\Sigma$  did not form a solid at seven days. Error bars represent standard deviation. Bar shading represents compressive strength calculation method.

sition are discussed later in Section 4. At 75 wt% BP-1, there are no identifiable trends when comparing between the  $0.3 \text{Si}/\Sigma$  (60 H<sub>2</sub>O),  $0.5 \text{Si}/\Sigma$  (60 H<sub>2</sub>O), and  $0.6 \text{Si}/\Sigma$  (60 H<sub>2</sub>O) composition series as the average CSs are within calculated uncertainty.

Lowering the water content of the activator solution to 45 wt% H<sub>2</sub>O leads to similar trends, as plotted in Fig. 10 B. A similar monotonic increase in CS with wt% BP-1 for

both the  $0.4 \text{Si}/\Sigma$  (45  $\text{H}_2\text{O}$ ) and  $0.5 \text{Si}/\Sigma$  (60  $\text{H}_2\text{O}$ ) composition series is measured. Notably, a lower activating solution water content of 45 wt%  $\text{H}_2\text{O}$  results in similar CS values for the  $0.5 \text{Si}/\Sigma$  composition series compared to the 60 wt%  $\text{H}_2\text{O}$  series (Fig. 11). Measurable geopolymer strength developed for the  $0.4 \text{Si}/\Sigma$  (45  $\text{H}_2\text{O}$ ) only at BP-1 wt% of 70 and 75, resulting in lower values as compared to the  $0.5 \text{Si}/\Sigma$  (45  $\text{H}_2\text{O}$ ) series.

#### 3.3.2. Nominal elemental ratios analysis of CS

Nominal elemental ratios (Si/Na, Si/Al, etc.) are commonly used to characterize the effect of changing geopolymer chemistry on material properties including CS, microstructure, Young's modulus, density, etc. for model geopolymer systems, typically derived from metakaolin (Silva et al., 2007, Duxson et al., 2005a, Duxson et al., 2007a). Plotting the material properties with nominal elemental ratios enables a common comparison across all data sets. The scaling of seven-day CS with relevant nominal molar ratios of Si, Al, Na, and water, are shown in Fig. 11.

The trends evident in Fig. 11 are that the seven-day CS varies monotonically with the nominal molar ratios examined within a given composition series. The CS monotonically increases with the nominal molar ratios of Si/Na and Si/H<sub>2</sub>O and decreases with Si/Al, trends generally consistent with the proximity of the samples' compositions to the ideal ratios as plotted in the pseudo-ternary state diagram (Fig. 2). It is important to note that these are nominal ratios based on the overall composition of each mixture and as such, do not necessarily reflect the elemental compositions of the binder phase formed.

#### 3.3.3. Strain to failure

Complementing the CS, the strain to fail provides indication of the brittle versus plastic behavior of the binders. The corresponding strain to failure of each composition is shown in Fig. 12. Excluding the  $0.3\text{Si}/\Sigma$  (60 H<sub>2</sub>O) samples,

it decreases with increasing BP-1 wt%, which indicates more brittle fracture behavior. The outlier behavior of the  $0.3 \mathrm{Si}/\Sigma$  (60 H<sub>2</sub>O) composition series shows nearly constant values with increasing BP-1 wt%. As with the trends for the CS, again the  $0.4 \mathrm{Si}/\Sigma$  sample series is differentiated by showing a more plastic behavior.

#### 3.3.4. Secant modulus

Secant moduli are plotted in Fig. 13 and the trends confirm the variations in behavior observed for the CS. The maximum measured secant modulus was  $147.34 \pm 37.66$  MPa for the 75 wt% BP-1  $0.3\text{Si}/\Sigma$  (60 H<sub>2</sub>O) geopolymer, coinciding with the maximum CS. For all composition series, the secant modulus increases with increasing BP-1 wt%. Comparing across composition series for the 60 wt% H<sub>2</sub>O compositions, the secant modulus decreases with increasing activating solution silica content with the exceptions of 55 wt% BP-1 group and the  $0.4\text{Si}/\Sigma$  series. For the  $0.4\text{Si}/\Sigma$  compositions, secant modulus values were greater for the 45 wt% H<sub>2</sub>O series compared to the 60 wt% H<sub>2</sub>O series at higher BP-1 wt%. Alternatively, in the  $0.5\text{Si}/\Sigma$  series, the 60 wt% H<sub>2</sub>O series obtained larger values of the secant modulus with the exception of 60 wt% BP-1 geopolymer.

# 3.3.5. Relationship between cube density and seven-day compressive strength

To test whether the observed variations in compressive strength were a consequence of imperfections in the cured cubes, the seven-day CS is plotted versus the seven-day

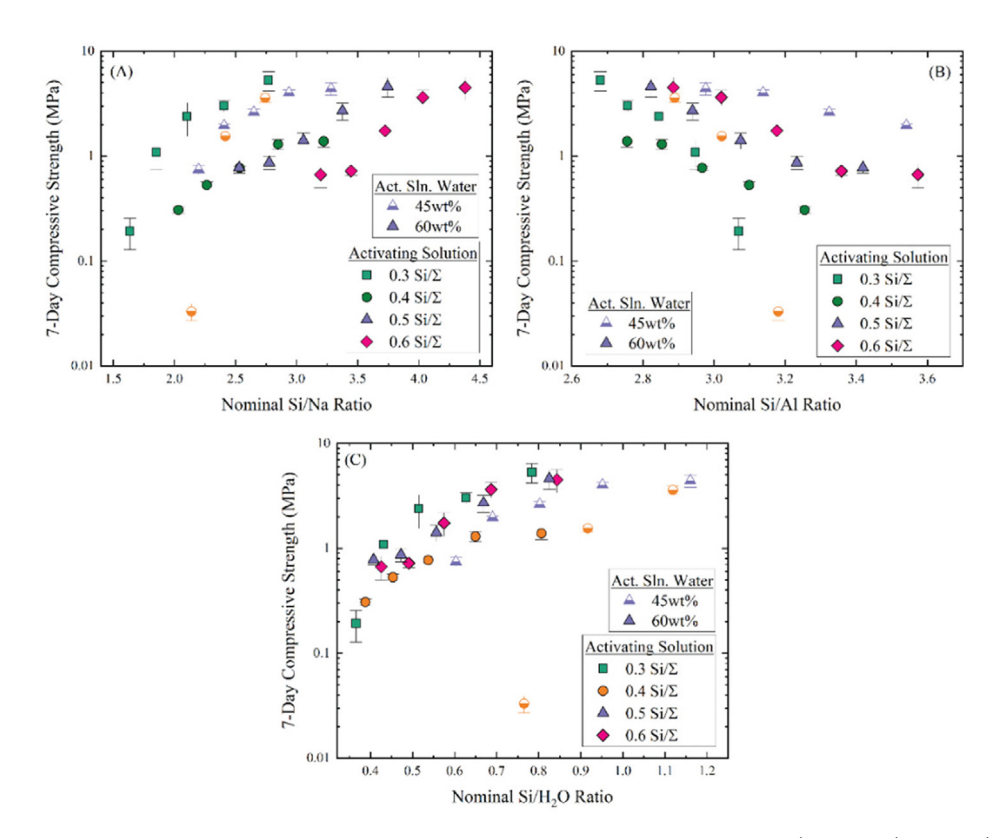


Fig. 11. Seven-day compressive strength versus nominal geopolymer molar ratios: (A) Si/Na (B) Si/Al (C) Si/H<sub>2</sub>O.

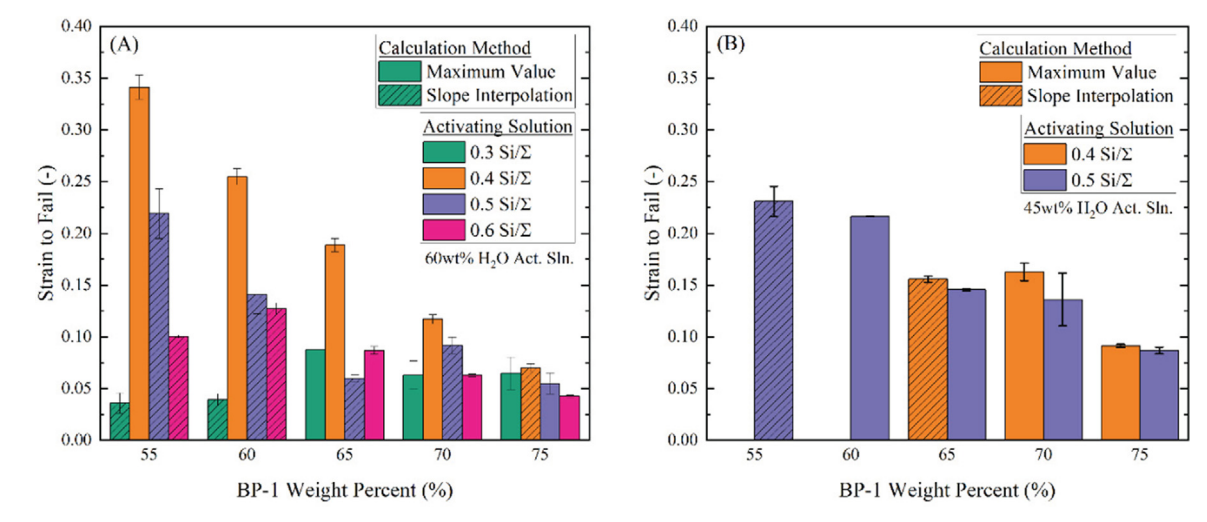


Fig. 12. (A) Strain to failure of BP-1 geopolymers of varying weight percents (55, 60, 65, 70, and 75) and varying  $Si/\Sigma$  nominal molar ratios (0.3, 0.4, 0.5, and 0.6) at an activating solution of 60 wt% water. Error bars represent standard deviation. Bar shading represents compressive strength calculation method. (B) Secant modulus of BP-1 geopolymers of varying weight percents (55, 60, 65, 70, and 75) at  $Si/\Sigma$  nominal molar ratios of 0.4 and 0.5 with an activating solution of 45 wt% water. Error bars represent standard deviation. Bar shading represents compressive strength calculation method.

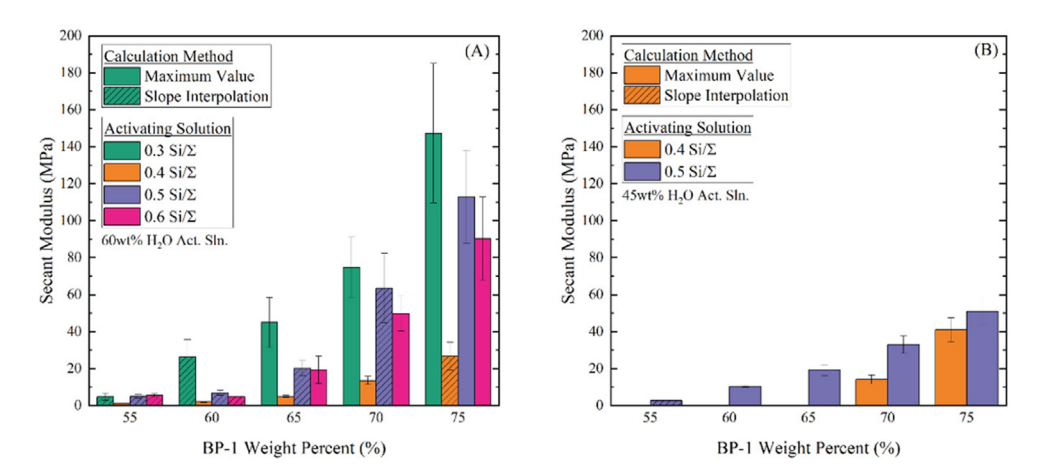


Fig. 13. (A) Secant modulus of BP-1 geopolymers of varying weight percents (55, 60, 65, 70, and 75) and varying  $Si/\Sigma$  nominal molar ratios (0.3, 0.4, 0.5, and 0.6) at an activating solution of 60 wt% water. Error bars represent standard deviation. Bar shading represents compressive strength calculation method. (B) Secant modulus of BP-1 geopolymers of varying weight percents (55, 60, 65, 70, and 75) at  $Si/\Sigma$  nominal molar ratios of 0.4 and 0.5 with an activating solution of 45 wt% water. Error bars represent standard deviation. Bar shading represents compressive strength calculation method.

cube density in Fig. 14 for 60 wt%  $H_2O$  activating solution geopolymers. With the exception of the  $0.4Si/\Sigma$  activating solution, there was no identifiable trend of CS with density or trends of density with any variable across composition series or within a composition series, which confirms that the variations in CS are not artifacts of the curing process, but rather reflect differences in underlying chemical and material properties. However, for the  $0.4Si/\Sigma$  activating solution the CS was anomalously low and the high density is due to significant water retention, as will be discussed further on has significant consequences for the geopolymer formed.

#### 3.4. Chemical structure (NMR)

Comparing differences in chemical coordination for geopolymers of varying composition, measured via solid-

state <sup>27</sup>Al and <sup>29</sup>Si NMR spectroscopy, provides additional information about the underlying molecular structure relationship between composition and material properties. All NMR measurements were conducted on geopolymers formed from 60 wt% H<sub>2</sub>O activating solutions.

# 3.4.1. <sup>27</sup>Al NMR

The  $^{27}$ Al spectra shown in Fig. 15 show a consistent peak at 60 ppm for all samples, representing four-coordinated aluminum (Engelhardt and Michel, 1987). Comparing geopolymer spectra to the BP-1 simulant spectra, there is no difference in peak location. No other aluminum peaks were present in the NMR spectra, e.g., a  $^{27}$ Al peak at  $\sim$  0 ppm correspond to six-coordinated aluminum (Duxson et al., 2005b, Hos et al., 2002). All aluminum in the binder phase originates from partial dissolution of the BP-1 regolith by the activating solution.

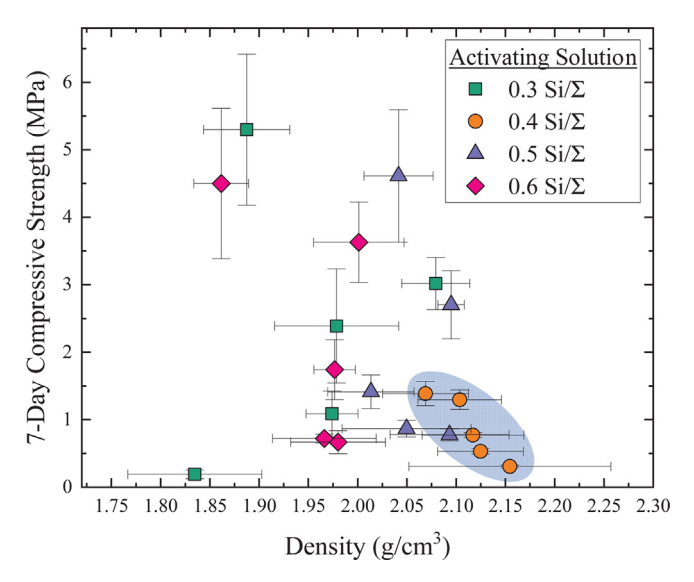


Fig. 14. Seven-day CS of all BP-1 geopolymer compositions created vs their density at 7 days. Error bars represent standard deviations. There are no visible trends in seven-day CS with cube density. Blue circle highlights the trend in CS with density identified for  $0.4\text{Si}/\Sigma$  activating solution geopolymers.

Following Lowenstein's rule, stating that Al-O-Al networks cannot form, all aluminum linkages in the samples are Al(4Si) (Löwenstein, 1954).

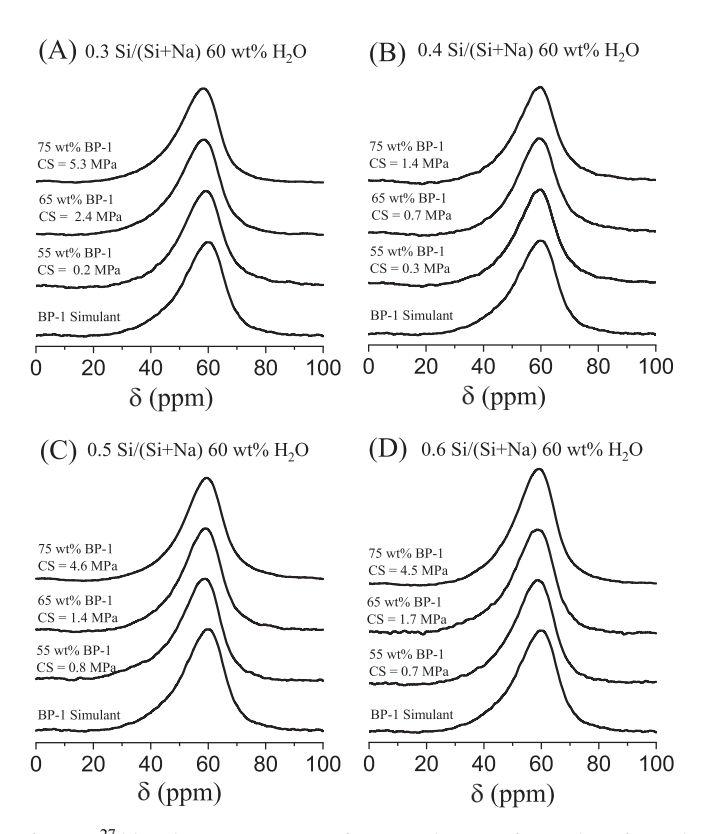


Fig. 15.  $^{27}Al$  MAS NMR spectra for geopolymers after 7 days formed from 60 wt%  $H_2O$  activating solutions: (A)  $0.3Si/\Sigma$  (60  $H_2O),$  (B)  $0.4Si/\Sigma$  (60  $H_2O),$  (C)  $0.5Si/\Sigma$  (60  $H_2O),$  and (D)  $0.6Si/\Sigma$  (60  $H_2O).$ 

# 3.4.2. <sup>29</sup>Si NMR

The  $^{29}$ Si NMR spectra (Fig. 16) display varying relative peak intensity with changes in BP-1 wt% and activating solution silica content (Si/ $\Sigma$  ratio). The  $^{29}$ Si spectra of all geopolymer samples show a broad hump from -80 to -110 ppm, spanning the well-defined Q<sup>4</sup>(mAl) range from -83 to -105 ppm and indicating a dominantly amorphous sample (Davidovits, 2020). Gaussian peak deconvolution is applied to define peaks corresponding to different silicon coordination (Fig. 17).

Fig. 16 shows that the 75 wt% BP-1 compositions for the  $0.3\text{Si}/\Sigma$  (60 H<sub>2</sub>O),  $0.5\text{Si}/\Sigma$  (60 H<sub>2</sub>O), and  $0.6\text{Si}/\Sigma$  (60 H<sub>2</sub>O) composition series are visually similar, with peak deconvolution showing that at the seven-day cure point, all five Q<sup>4</sup>(mAl) species are present in the 75 wt% BP-1 geopolymer <sup>29</sup>Si spectra. Relatively fewer lower-coordinated silica species are present for these formulations compared to those with lower wt% BP-1 (higher water content). Notably, the calculated Q<sup>4</sup>(0Al) relative content is the largest out of compositions studied in the 75 wt% BP-1  $0.3\text{Si}/\Sigma$  (60 H<sub>2</sub>O) geopolymer <sup>29</sup>Si spectra, the formulation which developed the highest compressive strength in this study.

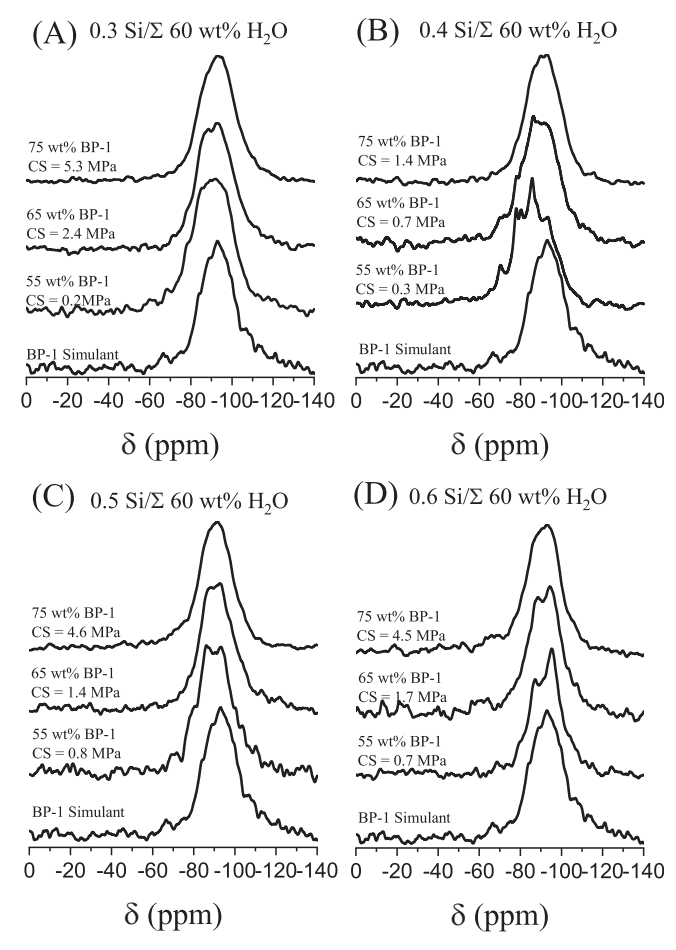


Fig. 16. <sup>29</sup>Si CP/MAS NMR spectra for geopolymers formed from 60 wt %  $H_2O$  activating solutions: (A)  $0.3Si/\Sigma$  (60  $H_2O$ ), (B)  $0.4Si/\Sigma$  (60  $H_2O$ ), (C)  $0.5Si/\Sigma$  (60  $H_2O$ ), and (D)  $0.6Si/\Sigma$  (60  $H_2O$ ).

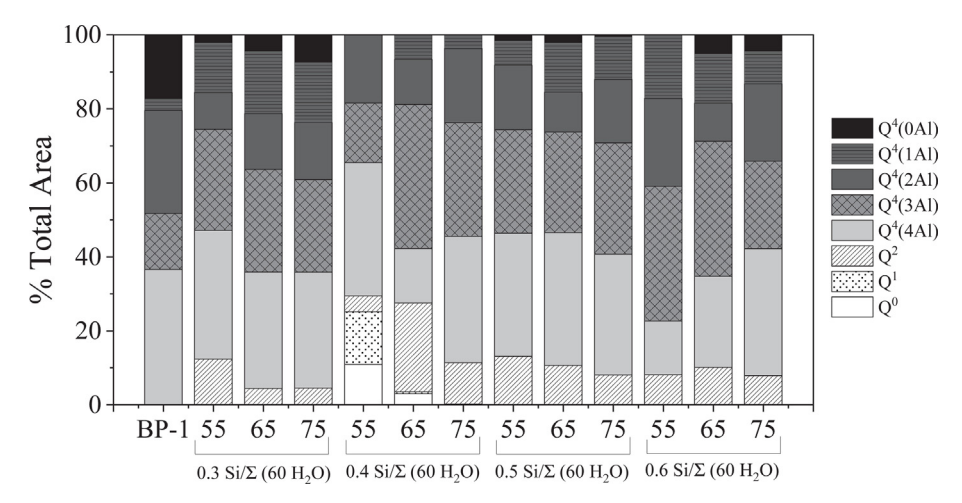


Fig. 17. Gaussian peak deconvolution of BP-1 simulant, 0.5Si/Σ (60 H<sub>2</sub>O) geopolymers, and 0.6Si/Σ (60 H<sub>2</sub>O) geopolymers at 55, 65, and 75 wt% BP-1 in formulation. Bottom axis excluding first column: Weight percent BP-1 in geopolymer formulation.

Differences in chemical coordination are most clearly observed as a function of composition when comparing the 55 wt% BP-1 spectra for each composition series. Fig. 16 shows that for the 0.4, 0.5, and  $0.6\text{Si}/\Sigma$  (60 H<sub>2</sub>O) composition series, primary peaks in the 55 wt% spectra shift from the  $Q^4(4AI)$  region at  $0.4Si/\Sigma$  to  $Q^4(3-4AI)$  at  $0.5 \text{Si}/\Sigma$  to Q<sup>4</sup>(2-3Al) at  $0.6 \text{Si}/\Sigma$ , supported by Fig. 17. This trend of more highly coordinated Si species at higher activating solution Si content confirms that as the reacting geopolymer incorporates more silicon into the binder gel at greater silica concentration in the activating solution as expected. However, there is no observable influence on compressive strength, likely due to the comparatively high water content in formulation. As BP-1 wt% increases, differences between spectra of different composition series become more difficult to distinguish until they become very similar at 75 wt% as previously mentioned.

Trends within a composition series are also observed. In the seemingly anomalous  $0.4\text{Si}/\Sigma$  (60 H<sub>2</sub>O) composition series, the 55 wt\% spectra show distinct peaks at -70, -77, and -80 ppm, indicating that significant amounts of less coordinated Si species  $(Q^0 - Q^2)$  are present after days of curing. Peak deconvolution seven attributes  $\sim 40 \%$  of overall peak area to these silica species at 55 wt% BP-1. These peaks remain at 65 and 75 wt% BP-1 but decrease in relative intensity with increasing BP-1 wt %. At 75 wt% BP-1, the  $0.4\text{Si}/\Sigma$  (60 H<sub>2</sub>O) composition is comprised primarily of O<sup>4</sup>(2-4Al), lacking a significant amount of  $Q^4(1A1)$  and absent of  $Q^4(0A1)$ . The presence of lower coordinated Si species  $(Q^0 - Q^2)$  indicates a reduced amount of reaction product formed in this composition series at seven days relative to the other composition series. As BP-1 wt% increases for the  $0.3\text{Si}/\Sigma$  (60 H<sub>2</sub>O) spectra deconvolutions show decreasing relative amounts of Q<sup>2</sup> and Q<sup>4</sup>(3Al) silicon coordination along with increasing  $Q^4(0Al)$  and  $Q^4(2Al)$  sites.

The connection between material property differences seen in Section 3.2 and chemical coordination differences is further discussed in the Discussion (Section 4).

#### 3.5. Water content

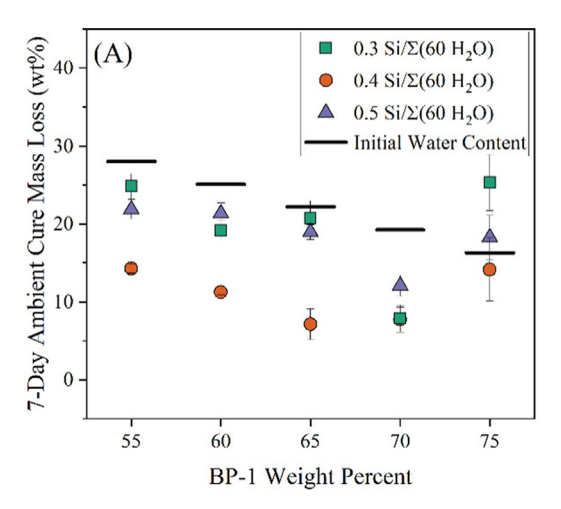
Water content data for geopolymer compositions at the seven-day cure point are included in Table A3 in the Appendix.

# 3.5.1. 60 wt% $H_2O$ activating solutions

Fig. 18A shows percent mass loss during curing of all compositions measured (0.3, 0.4, and  $0.5 \mathrm{Si}/\Sigma$  (60 H<sub>2</sub>O)). Mass loss is due to the evaporation of water from the geopolymer sample after the polycondensation reaction responsible for binder formation proceeds as geopolymerization is water neutral. Mass loss trends are non-monotonic within a given composition series.

Geopolymers formed from the  $0.4\mathrm{Si}/\Sigma$  (60  $\mathrm{H}_2\mathrm{O}$ ) activating solution retain significantly more mass after seven days of ambient curing compared to geopolymers formed from  $0.3\mathrm{Si}/\Sigma$  (60  $\mathrm{H}_2\mathrm{O}$ ) and  $0.5\mathrm{Si}/\Sigma$  (60  $\mathrm{H}_2\mathrm{O}$ ) activating solutions. This result supports the observations from the NMR results, specifically that unreacted soluble silicates are still present in the  $0.4\mathrm{Si}/\Sigma$  (60  $\mathrm{H}_2\mathrm{O}$ ) geopolymers after seven days of curing. The presence of unreacted soluble silicates, as indicated by <sup>29</sup>Si NMR results of the  $0.4\mathrm{Si}/\Sigma$  composition, retains more mass in the geopolymer cubes as water mass cannot leave the system via evaporation until the polycondensation reaction occurs releasing water. This anomalous behavior in water retention correlates with the anomalously poor CS of samples formed from this activator composition.

The 75 wt% BP-1  $0.3 \text{Si}/\Sigma$  (60  $\text{H}_2\text{O}$ ) composition has a calculated mass reduction greater than the original calculated mass of water in formulation for the  $0.3 \text{Si}/\Sigma$  (60  $\text{H}_2\text{O}$ ) geopolymer. Increased mass reduction could be due to the release of sodium from the system that was not required to balance charge within the developing aluminosilicate binder network, as the  $0.3 \text{Si}/\Sigma$  (60  $\text{H}_2\text{O}$ ) composition has a significantly higher Na/Al and Na/Si ratio. As mentioned in Section 3.1.2, a coating of white powder was observed on the surface and sides of the 75 wt% BP-1 0.3Si/



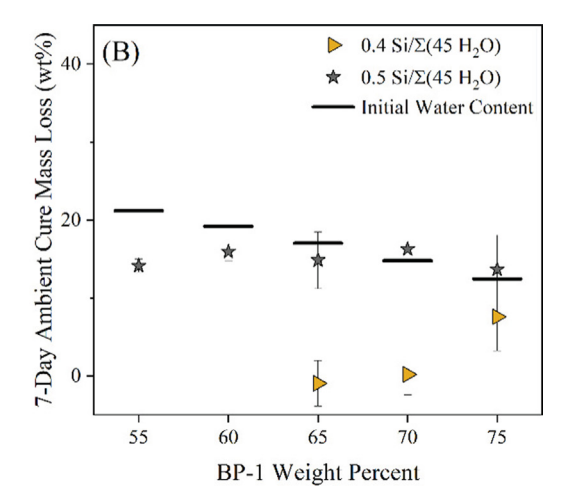


Fig. 18. Weight % of initial activated BP-1 solution lost to the environment during ambient curing over seven days for (A) geopolymers formed from 60 wt %  $H_2O$  activating solutions and (B) 45 wt%  $H_2O$  activating solutions. Data for 55 and 60 wt% compositions of  $0.4Si/\Sigma$  (45  $H_2O$ ) does not exist as the composition did not form solid cubes at seven days. The mass wt% of water originally in each composition is shown in black dashes.

 $\Sigma$  (60 H<sub>2</sub>O) cubes which likely led to mass remaining in the cube mold after curing, leading to a calculated mass loss greater than the initial water mass. Seven percent of cube mass was lost for this composition that cannot be attributed to water loss, within the mass of sodium and silica added (10 wt%). This observation corresponds with observations from studies on metakaolin-derived geopolymers which noted the presence of sodium carbonate formed along with the final geopolymer product (Barbosa et al., 2000). Mass loss calculations are also potentially convoluted by geopolymer residue stuck to the silicone molds remaining after removing the cubes.

# 3.5.2. 45 wt% $H_2O$ activating solutions

Fig. 18B shows that almost no mass is lost after seven days of curing for geopolymer compositions formed with  $0.4\text{Si}/\Sigma$  (45 H<sub>2</sub>O) activating solution, following a similar trend to the  $0.4\text{Si}/\Sigma$  (60 H<sub>2</sub>O) in Fig. 18A. Almost no mass is lost to the environment for the 65 and 70 wt% BP-1 compositions, followed by increased mass reduction at the 75 wt% BP-1 composition. Again, the  $0.4\text{Si}/\Sigma$  activator composition yields geopolymers with anomalously low CS. The  $0.5\text{Si}/\Sigma$  (45 H<sub>2</sub>O) composition shows a constant mass loss value at  $\sim$  15 wt% across the entire composition series.

#### 4. Discussion

# 4.1. Composition-property relationships of BP-1 geopolymers

The first objective, namely determining how formulation composition affects geopolymer properties, reveals that the greatest average seven-day CS is achieved for the system with high BP-1 wt% (75 wt%), highest activating solution water content (60 wt%  $H_2O$ ), and the lowest Si content (0.3Si/ $\Sigma$ ). The nominal composition of this system, shown in Fig. 2, lies close to the suggested optimal Na/Al = 1

ratio and is closest to the optimal ratio of Si/Al = 2 (both given as the dashed lines in Fig. 2). It is reassuring that the nominal composition closest to the intersection of these two compositional guides on the pseudo-ternary diagram yielded the strongest geopolymer as judged by both the CS and the secant modulus. However, we do not see a uniform decrease in CS as the nominal elemental composition moves away from this optimal point, as was originally hypothesized. This sample also showed a seemingly anomalous mass loss that is attributed to water evaporation and convective loss of sodium as similarly observed for metakaolin geopolymers formed with excess cation in formulation (He et al., 2016, Barbosa et al., 2000).

The seven-day CS values for the 75 wt% BP-1 geopolymer compositions are the most significant as the 0.3, 0.5, and  $0.6\text{Si}/\Sigma$  (60 H<sub>2</sub>O) compositions displayed the highest CS within overlapping error bars. <sup>29</sup>Si NMR results show a relatively greater amount of Si enriched sites (Q<sup>4</sup>(1Al), Q<sup>4</sup>(2Al), and Q<sup>4</sup>(3Al)) (Fig. 17) for compositions that formed higher CS at seven days similar to literature results for fly ash geopolymers (Fernández-Jiménez et al., 2006). These high strength compositions contained minimal measurable Si species (Q<sup>0</sup> – Q<sup>3</sup>) species indicating that available Si has been incorporated into the geopolymer gel binder, supported by mass loss values indicating almost complete evaporation of water from the system.

A surprising deviation from the overall trends of increasing CS with BP-1 content and Si/H<sub>2</sub>O ratio is observed for samples derived from the 0.4Si/Σ activating solutions, replicated for three independent trials. These samples show the lowest strengths and do not form brittle solids but rather deform plastically and retain high water content. <sup>29</sup>Si NMR shows these samples lack the highly coordinated Q<sup>4</sup>sites, showing a higher fraction of lower coordinated Si silica. As mentioned in the background, similar fluctuating CS trends were observed in fly-ash geopolymers formed from activating solutions with systematically varied Na<sub>2</sub>SiO<sub>3</sub>/NaOH content (Al Bakri Abdullah

Table 6
Comparison of launch mass for geopolymer and concrete to form 1 m<sup>3</sup> of structure.

Material Components	Mass required for 1 m <sup>3</sup> of structure (kg/m <sup>3</sup> )
Solid Components of Geopolymer Activating Solution	252
Cement (solids)	400

et al., 2012). The difference in activating solution composition resulting in the anomalous CS decrease (Si/ $\Sigma$  values of 0.2 - 0.22 in their study and  $0.4\text{Si}/\Sigma$  in this study) is likely due to the variation in composition between the BP-1 regolith simulant and fly ash as the fly ash contained 5 % more  $SiO_2$  and 7 % more  $Al_2O_3$  by mass. The presence of  $Q^0$ - $Q^3$ sites at long times after mixing (Fig. 17) indicates that sodium silicate is not being consumed to form the geopolymer gel binder, resulting in comparable weaker CS when compared to geopolymers that form primarily Q<sup>4</sup> highly Al substituted units (Barbosa et al., 2000). Water content results after curing support this conclusion, showing reduced mass loss for the  $0.4\text{Si}/\Sigma$  (60 H<sub>2</sub>O) composition when compared to the 0.3 and  $0.5\text{Si}/\Sigma$  compositions at both levels of water content (45 and 60 wt% H<sub>2</sub>O activating solutions). As mentioned in Section 3.5.1, unreacted silicate species result in less water formed during the polycondensation reaction to form the geopolymer binder gel network, translating to reduced mass loss during curing. Identification of such significant deviations for specific chemical compositions is critically important for avoiding serious problems in geopolymer manufacturing.

Observed differences in seven-day chemical coordination may be due to differences in the distribution of silicate species in the activating solution. Provis et. al showed that in sodium silicate solutions formed from the same materials as this study produced dominantly monomeric Q<sup>0</sup> Si coordinated sites at low SiO<sub>2</sub>/Na<sub>2</sub>O ratios (less than 1), and a mixture of higher order Q<sup>2</sup> and Q<sup>3</sup>Si sites at high SiO<sub>2</sub>/ Na<sub>2</sub>O ratios (greater than 1.75) (Provis et al., 2005). The equivalent SiO<sub>2</sub>/Na<sub>2</sub>O ratios for activating solutions in this study ranged from 0.85  $(0.3Si/\Sigma)$  to 3  $(0.6Si/\Sigma)$ , predicting a significant difference in activating solution speciation. A greater amount of monomeric silica species has been linked to increased dissolution of the aluminosilicate source and the rapid formation of an Al-rich gel, while bulky higher order Si species may remain unreacted at early times and later incorporate into the geopolymer gel (Provis and Van Deventer, 2007, Rees et al., 2007). This phenomenon is supported by the 55 wt% BP-1 <sup>29</sup>Si NMR spectra which show more highly Si coordinated Q<sup>4</sup> species at higher activating solution Si content (0.5 and 0.6Si/ $\Sigma$ ). Duxson et. al also showed that higher silica concentration led to microstructural changes including smaller pores in the gel phase and greater densification of the geopolymer gel (Duxson et al., 2005a). In this work, the  $0.4\text{Si}/\Sigma$  activating solution, existing at an equivalent SiO<sub>2</sub>/Na<sub>2</sub>O ratio of 1.3, may not have enough monomeric silica to induce rapid dissolution while also containing less highly coordinated silica

species in solution to form a dense silica-rich gel at seven days. However, further kinetic studies and <sup>29</sup>Si NMR measurements of the activating solutions in this study are needed to confirm this hypothesis.

Combined molar ratio analysis and NMR characterization suggests that the nominal Si/H<sub>2</sub>O ratio is the main determinant of seven-day CS development for BP-1 geopolymers formed at relatively high water content (Si/  $H_2O < 0.6$ ), after which variations in chemical structure at low water content (Si/H<sub>2</sub>O > 0.6) results in significant CS differences. Fig. 11C supports this observation when combined with the chemical coordination analysis from <sup>29</sup>Si NMR. Geopolymers with the highest CS (0.3Si/Σ (60  $H_2O$ ),  $0.5Si/\Sigma$  (60  $H_2O$ ),  $0.6Si/\Sigma$  (60  $H_2O$ )) all display larger relative amounts of highly silica substituted Q<sup>4</sup>(1-3Al) compared to the weaker  $0.4\text{Si}/\Sigma$  (60 H<sub>2</sub>O). Similar <sup>29</sup>Si NMR observations in metakaolin (Kim, 2012, Duxson et al., 2005a) and fly ash (Fernández-Jiménez et al., 2006) based geopolymers show increased CS with a greater proportion of Si-O-Si bonds formed. These results provide clear evidence for objective two (to connect empirically trends in CS of the BP-1 geopolymers with chemical structure of the geopolymer gel binder), whereby superior geopolymer CS is correlated with more Si-O-Ai linkages in the gel binder, which itself is promoted by formulation composition.

The higher CS developed by ambiently cured geopolymers at lower water content is supported by results for compositionally similar fly ash geopolymer systems (Barbosa et al., 2000, Hardjito et al., 2004b, Hardjito et al., 2004a, Xie and Kayali, 2014) and metakaolin geopolymers (Vitola et al., 2020). Maximum strength attained in this study at a 0.15 H<sub>2</sub>O/solids ratio agrees well with the ratio of 0.17 observed by Hardjito et. al for fly ash geopolymers but is significantly lower than the 0.22 optimal ratio from Xie and Kayali, potentially due to 0.22 being the lower limit of their investigation. Water is a reactant in the dissolution reactions responsible for releasing silicate and aluminate ions from BP-1, facilitates ion transfer, and is a product of the polycondensation reaction responsible for forming the geopolymer binder gel (Weng and Sagoe-Crentsil, 2007). At high water content, the polycondensation reaction step is limited by the high concentration of water in solution, following Le Chatlier's principle, resulting in less gel binder formation and lower seven-day CS. As noted by Zuhua et al. for metakaolin based geopolymers, residual water suppressed the polycondensation reaction and resulted in decreased CS, specifically when the OH<sup>-</sup> concentration is greater than 12 mol/L (Zuhua et al., 2009).

#### 4.2. Comparison to basalt geopolymer systems

Ambient-cure CS values for BP-1 geopolymers in this study (5.3  $\pm$  1.1 MPa) were in the range of CS values for geopolymers formed from terrestrial basalt (Saraya and El-Fadaly, 2017, Mao et al., 2022). While direct comparison of seven-day CS results is not possible due to nonstandardized precursor particle size, activating solution, and curing protocol, similar CS values were obtained for Saraya et al. activating terrestrial basalt with sodium hydroxide and water (4–12 MPa) and Mao with activating basalt with sodium silicate and NaOH (2.4 MPa). The CS values for BP-1 geopolymers in this study, however, are lower than those determined by Mills et. al (9.4 MPa) despite identical curing protocols and sieving protocol of the BP-1 simulant (Mills et al., 2022b). This discrepancy is likely due to the different form of sodium silicate activating solution used. Mills et. al formed BP-1 geopolymers at 71 wt% BP-1 using a commercially available sodium silicate solution (37 wt%, Sigma Aldrich) as opposed to creating the activating solution from water, fumed silica, and sodium hydroxide as done in this study to precisely control activating solution composition. The choice of sodium silicate precursor is known to affect the resulting properties of a geopolymer, even if the nominal elemental ratio if the activating solutions is identical (Sagoe-Crentsil and Weng, 2006).

# 4.3. Considerations for lunar ISRU

# 4.3.1. Optimization of resources for lunar ISRU

Optimizing geopolymer composition for lunar ISRU requires minimization of material transported from Earth to the lunar surface while maintaining desired material properties. Assuming that water is available at the lunar surface, sodium hydroxide and fumed silica are the only two components that need to be sourced from Earth. The strongest geopolymer found in this study was  $5.3 \pm 1.12$ MPa, from the 75 wt% BP-1  $0.3\text{Si}/\Sigma$  (60 H<sub>2</sub>O) composition. Importantly, this composition only requires 25 wt% activating solution. To create the activating solution for 1 m<sup>3</sup> of this geopolymer, 377 kg of liquid water, 153 kg of solid NaOH, and 99 kg of solid SiO<sub>2</sub> are required for a total of 629 kg/m<sup>3</sup>. The geopolymerization reaction is net water neutral and is not consumed in the reaction (Davidovits, 2020). Because of this, reclaiming water used to form the geopolymer has been reported by Wang et. al. up to 98.61 % (Wang et al., 2017). A full recycling system of water would decrease the launch mass to 252 kg/m<sup>3</sup>. This is a significant reduction compared to the mass required for traditional concrete, seen in Table 6 (Mindess, 2019).

#### 4.3.2. Additional considerations for compressive strength

The lunar environment presents a greater engineering challenge with atmospheric pressures close to vacuum, decreased protection from solar radiation, and thermal cycling from -223 to -71 °C at the poles (Williams et al.,

2017). Geopolymers formed from aluminosilicate sources including BP-1 were shown to have reduced CS when cured under vacuum and no solid geopolymer formation when cured at sub-zero temperatures (Mills et al., 2022b). A viable geopolymer construction method for the lunar surface will need to address such environmental limitations to geopolymer strength formation. Additional experimental techniques could also be applied to increase the CS of these materials. Examples include decreasing the average particle size through milling or other methods (Jamkar et al., 2013), alkali fusion to increase the reactivity (Mao et al., 2022), and alternate heating procedures such as traditional convection, microwave radiation, or some combination (Shi et al., 2020, Rovnaník, 2010). With the inclusion of any of these additional procedures, additional energy usage and equipment requirements must be considered. All properties investigated in this study were at seven days, although these properties evolve with time. A greater understanding of the kinetics of these systems and how they relate to various intermediate and final material properties would be extremely valuable for optimization of geopolymers for lunar ISRU.

#### 5. Conclusions

The objectives of this study were to (1) measure material properties of BP-1 lunar regolith simulant geopolymers of varying composition and determine trends for strength development based on varying composition, and then, (2) validate that these trends seen empirically in the compressive strength measurements of the BP-1 geopolymers are due to variations in the chemical structure of the geopolymer gel binder. Geopolymer compositions explored varying regolith simulant weight percent (55 to 75 wt% BP-1), activating solution sodium and silicon content ((Si/ Si + Na) ratios of 0.3 to 0.6), and activating solution water content (45 and 60 wt% H<sub>2</sub>O). The main observations of our work are as follows: Compressive strength, strain to fail, and secant modulus were found to be nontrivial functions of varying activating solution formulation following a standardized curing protocol. Increasing the mass fraction of the BP-1 simulant in formulation resulting in increased compressive strength, greater secant modulus, and decreased strain to fail for all studied composition series (formed from the same activating solution). Residual water present at higher activating solution mass fractions suppresses the polycondensation reaction responsible for forming the gel binder phase of the geopolymer, agreeing with the wider geopolymer literature. Importantly, within each composition series, geopolymers formed the highest compressive strength at a BP-1 simulant weight percent of 75 % for all activating solution compositions. Of all compositions studied, the highest average seven-day CS is achieved for the composition with high BP-1 wt% (75 wt %), highest water content (60 wt% in activating solution), and the lowest Si content  $(0.3\text{Si}/\Sigma)$ . This result can be understood by plotting the nominal formulations on the

pseudo-ternary state diagram (Fig. 2), where it is evident that the highest compressive strengths were achieved by samples closest to the idealized ratios of Si/Al = 2 and Na/Al = 1 (as previously identified in the literature). A seemingly anomalous decrease in compressive strength was observed for the  $0.4\text{Si}/\Sigma$  (60 H<sub>2</sub>O) composition series. Differences in chemical coordination showed that lower coordinated silicon species were still present in  $0.4\text{Si}/\Sigma$ (60 H<sub>2</sub>O) geopolymers after seven days of curing along with greater water retention, indicating that the polycondensation reaction responsible for gel binder strength was suppressed for this composition. Identification of significant differences in Si and Al coordination of the geopolymer gel binder at the molecular level contributing to this critical deviation in trends between CS and nominal formulation provides additional guidance for the rational design of superior geopolymer construction materials and warrants additional investigation.

Comparison of our results for BP-1 with literature show CS in range of ambiently cured basalt geopolymers, similar observations of increasing geopolymer strength with increasing Si enriched sites (Q<sup>4</sup>(1Al), Q<sup>4</sup>(2Al), and Q<sup>4</sup>(3Al)) in the gel binder, and similar non-monotonic trends in CS with varying activator Si/ $\Sigma$  ratio to fly-ash geopolymer studies. Further research studying geopolymer rheology, reaction kinetics, and strength development time-scales of interest may build on the relationships determined

in this study, which should find utility in technological applications including additive manufacturing.

#### **Declaration of Competing Interest**

The authors declare that they have no known competing financial interests or personal relationships that could have appeared to influence the work reported in this paper.

# Acknowledgements

This manuscript was prepared based upon work supported by the National Science Foundation DMREF (No. 2118944) and under cooperative agreement #70NANB20H133 from NIST, U.S. Department of Commerce. This publication was also made possible by the Delaware COBRE program through the use of NMR cores, supported by a grant from the National Institute of General Medical Sciences – NIGMS (5 P30 GM110758-02) from the National Institutes of Health. The authors would also like to thank Caitlin Quinn for assistance with NMR data collection, Raul Lobo for insightful conversations, and NASA Kennedy Space Center for supplying the BP-1 regolith simulant material.

# **Appendix.** See Figs. A1-A10 and Tables A1-A3.

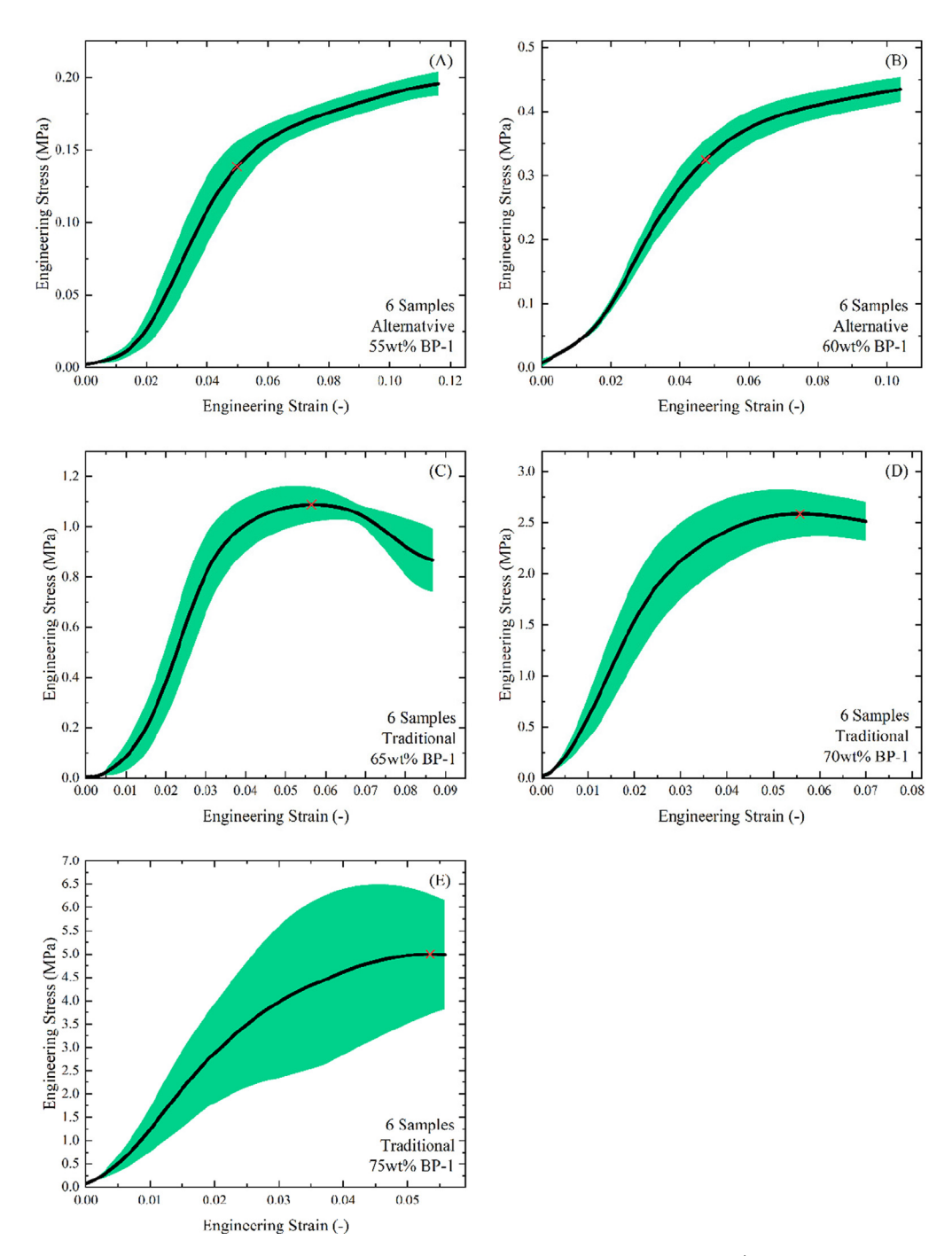


Fig. A1. Average engineering stress vs. engineering strain curves of BP-1 geopolymers, created with the  $0.3\text{Si}/\Sigma$  (60 H<sub>2</sub>O) activating solution, after 7 days of curing at ambient temperature and pressure. The green band represents  $\pm$  1 standard deviation and the red X indicates compressive strength and corresponding strain. The number of samples measured for each composition is indicated on the graph along with calculation method for compressive strength.

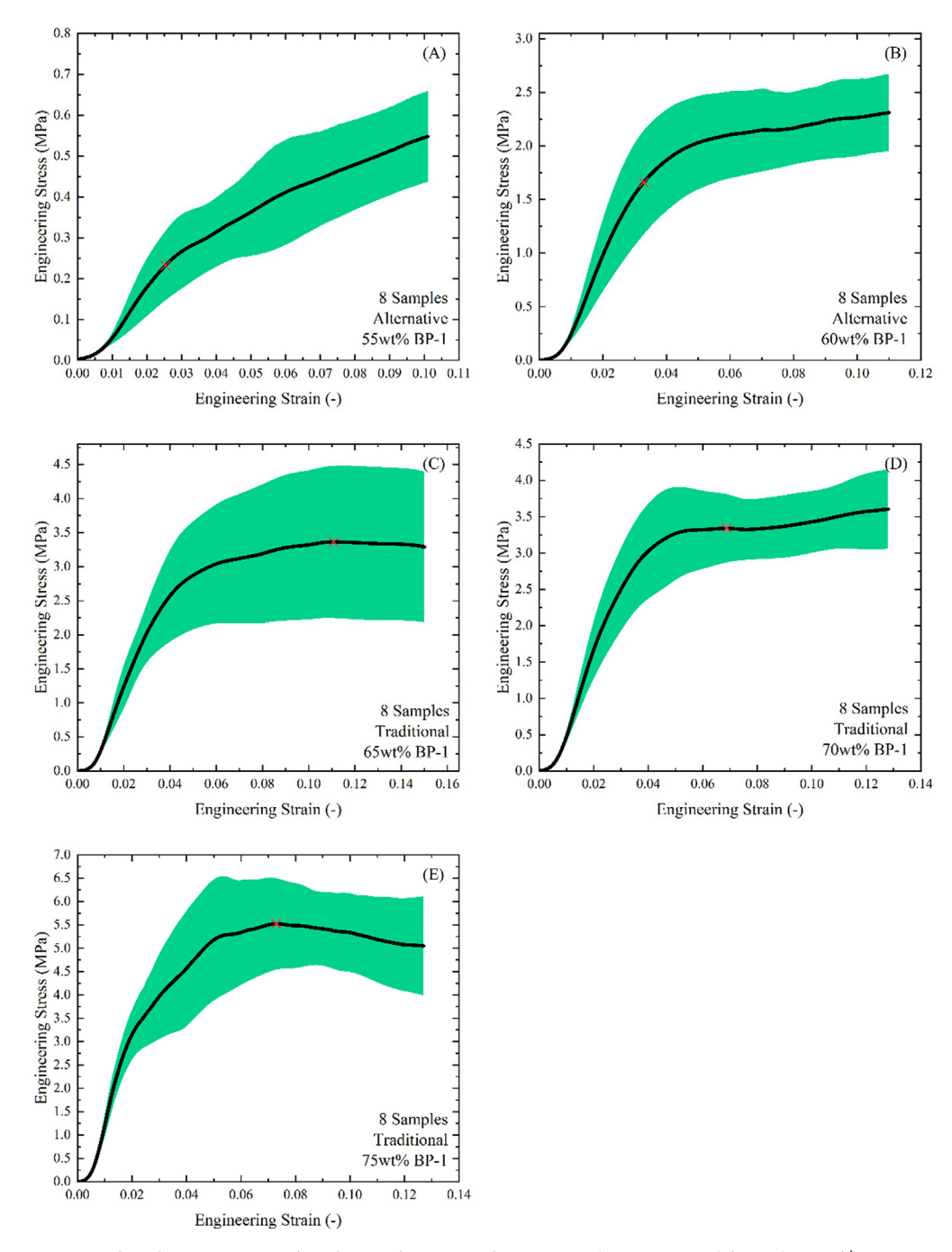


Fig. A2. Replicate average engineering stress vs. engineering strain curves of BP-1 geopolymers, created from the  $0.3\text{Si}/\Sigma$  (60  $\text{H}_2\text{O}$ ) activating solution, after 7 days of curing at ambient temperature and pressure. The green band represents  $\pm$  1 standard deviation and the red X indicates compressive strength and corresponding strain. The number of samples measured for each composition is indicated on the graph along with calculation method for compressive strength.

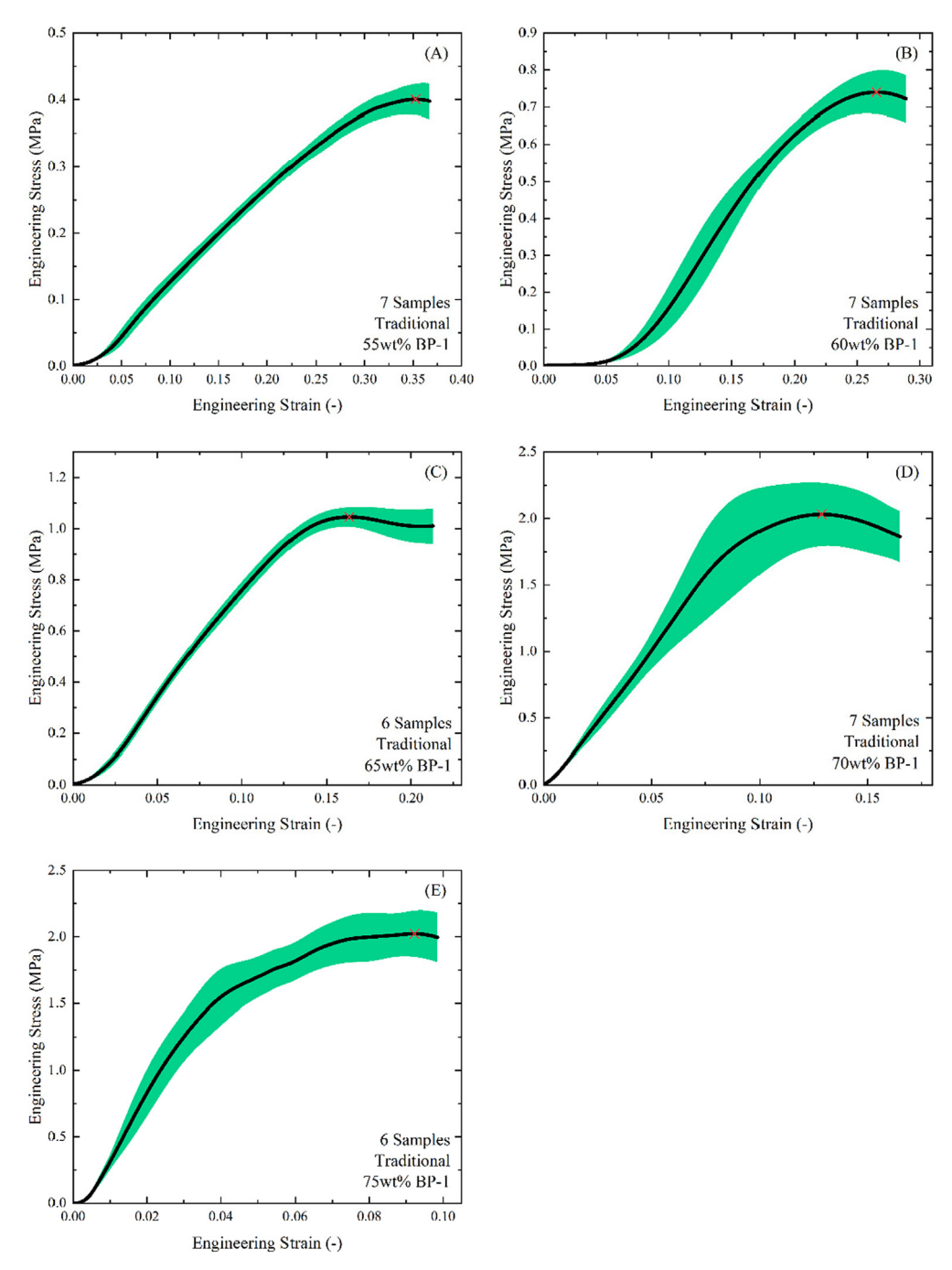


Fig. A3. Average engineering stress vs. engineering strain curves of BP-1 geopolymers, created from the  $0.4\text{Si}/\Sigma$  (60 H<sub>2</sub>O) activating solution, after 7 days of curing at ambient temperature and pressure. The green band represents  $\pm$  1 standard deviation and the red X indicates compressive strength and corresponding strain. The number of samples measured for each composition is indicated on the graph along with calculation method for compressive strength.

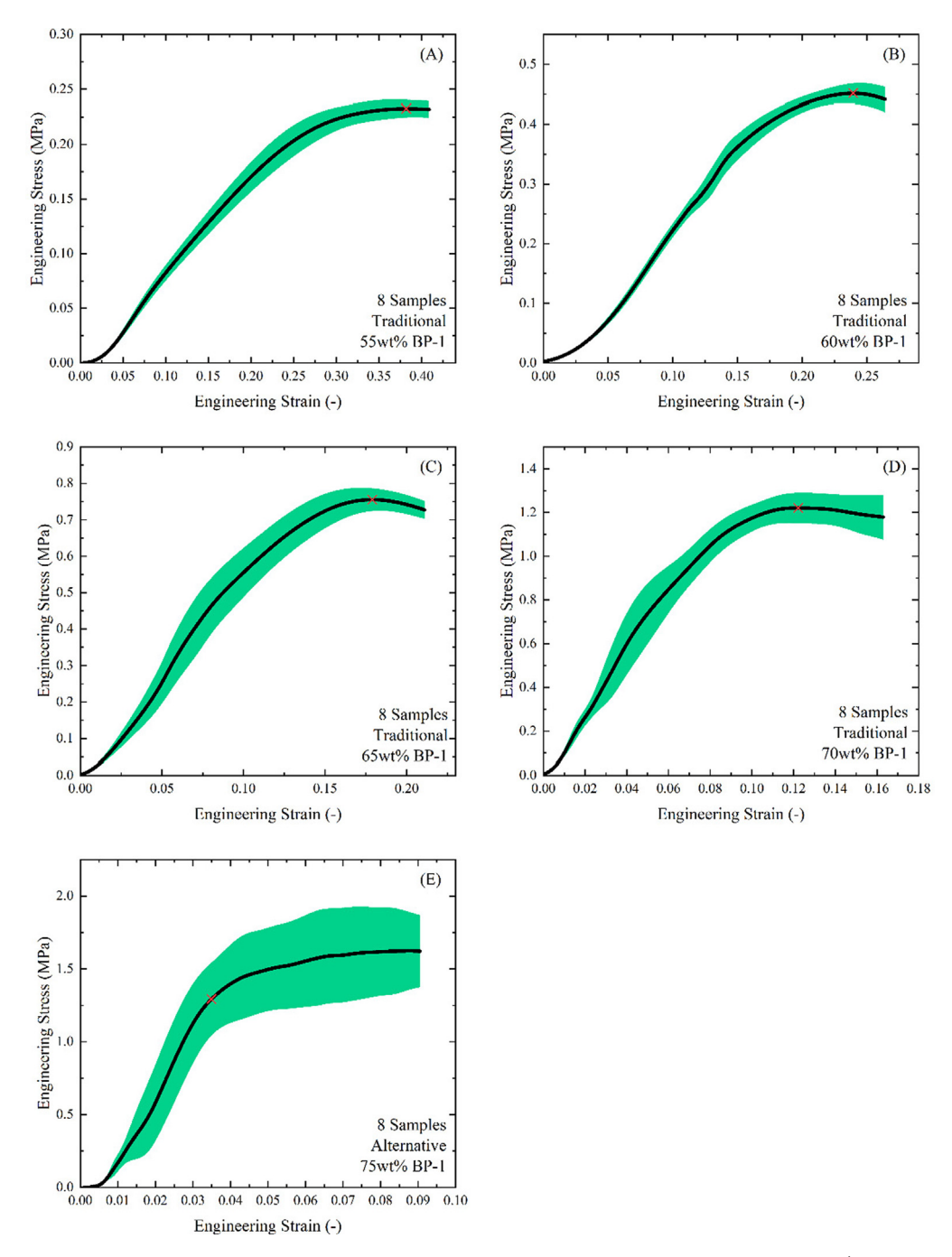


Fig. A4. Replicate average engineering stress vs. engineering strain curves of BP-1 geopolymers, created from the  $0.4\text{Si}/\Sigma$  (60  $\text{H}_2\text{O}$ ) activating solution, after 7 days of curing at ambient temperature and pressure. The green band represents  $\pm$  1 standard deviation and the red X indicates compressive strength and corresponding strain. The number of samples measured for each composition is indicated on the graph along with calculation method for compressive strength.

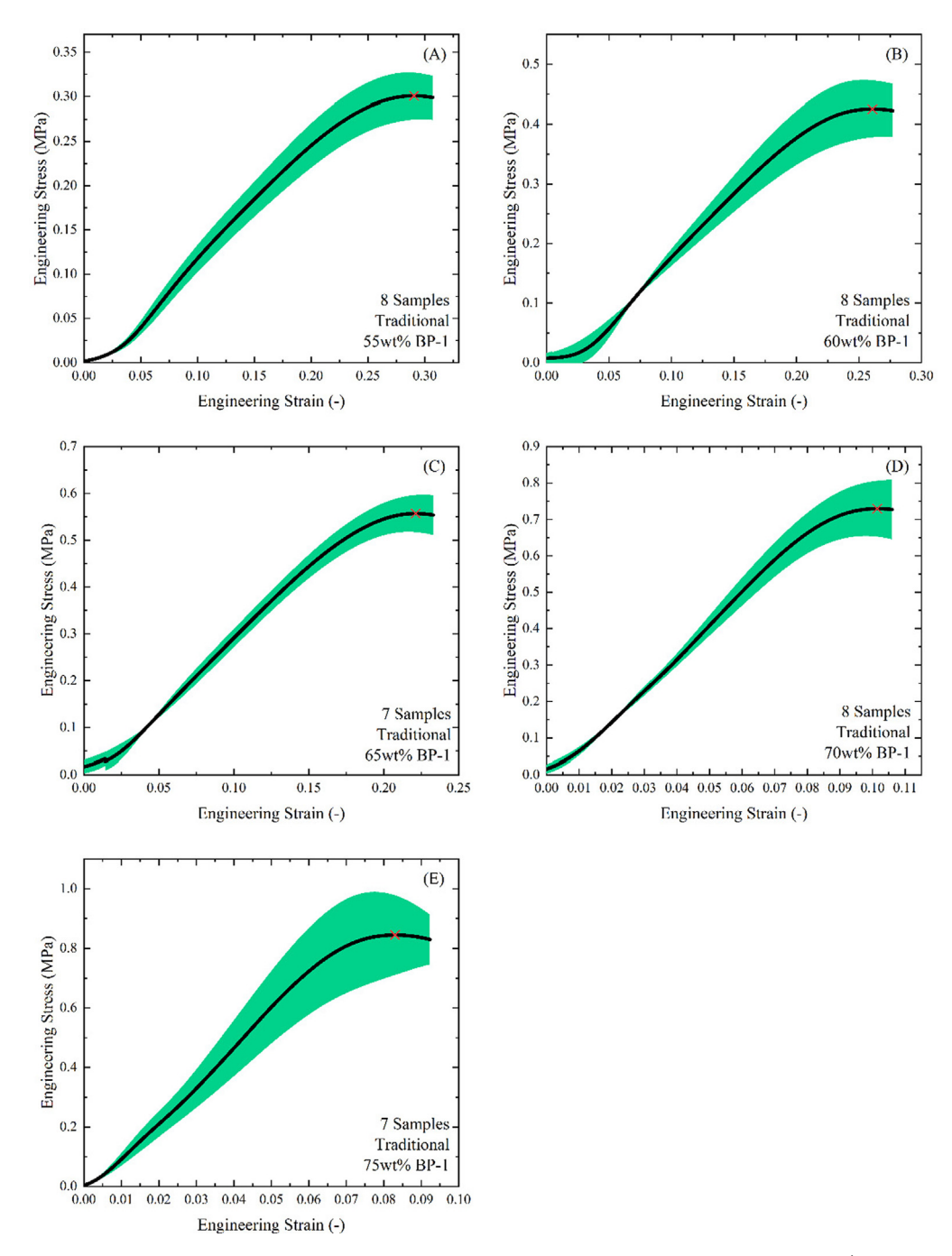


Fig. A5. Replicate average engineering stress vs. engineering strain curves of BP-1 geopolymers, created from the  $0.4\text{Si}/\Sigma$  (60  $\text{H}_2\text{O}$ ) activating solution, after 7 days of curing at ambient temperature and pressure. The green band represents  $\pm$  1 standard deviation and the red X indicates compressive strength and corresponding strain. The number of samples measured for each composition is indicated on the graph along with calculation method for compressive strength.

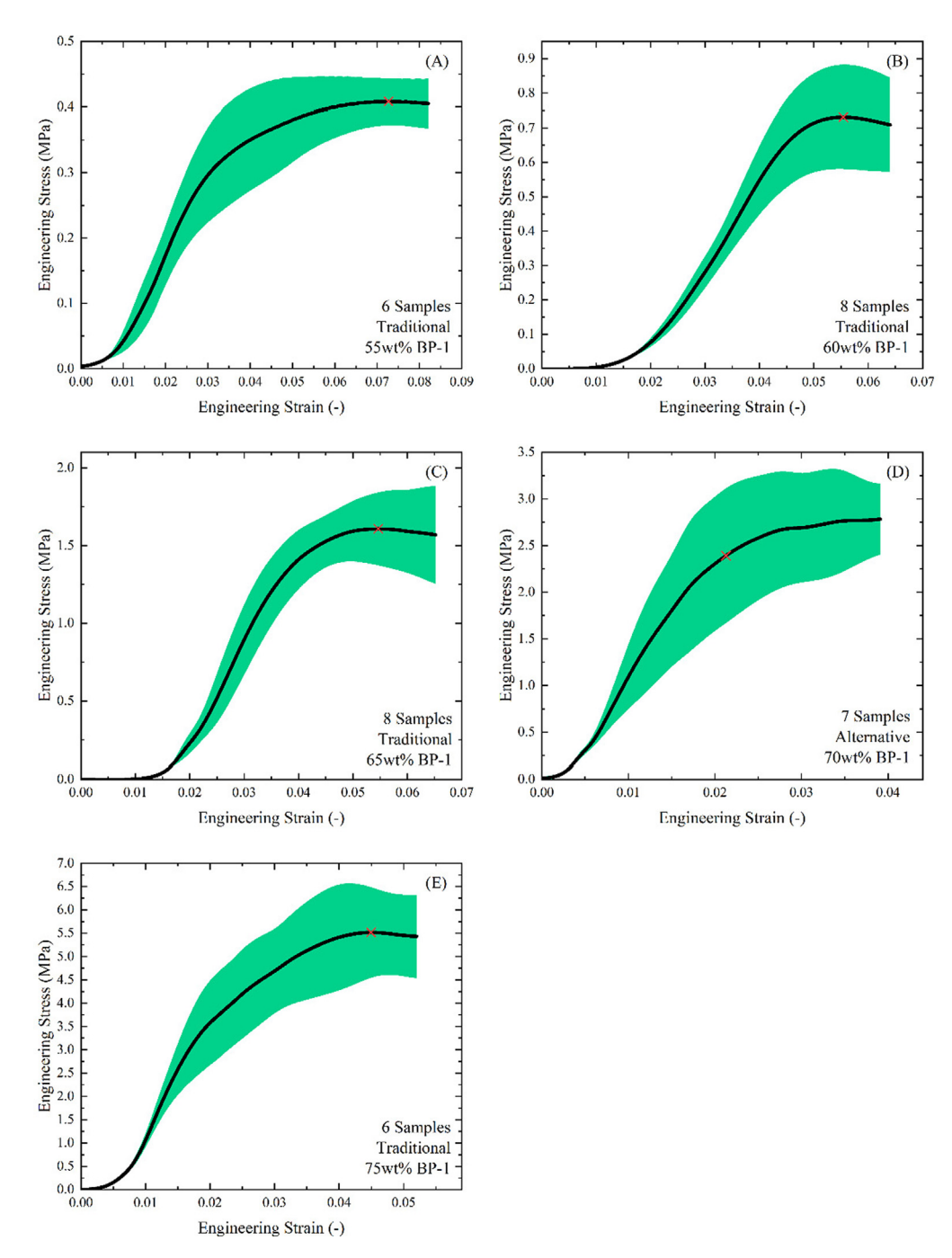


Fig. A6. Average engineering stress vs. engineering strain curves of BP-1 geopolymers, created from the  $0.5\text{Si}/\Sigma$  (60 H<sub>2</sub>O) activating solution, after 7 days of curing at ambient temperature and pressure. The green band represents  $\pm$  1 standard deviation and the red X indicates compressive strength and corresponding strain. The number of samples measured for each composition is indicated on the graph along with calculation method for compressive strength.

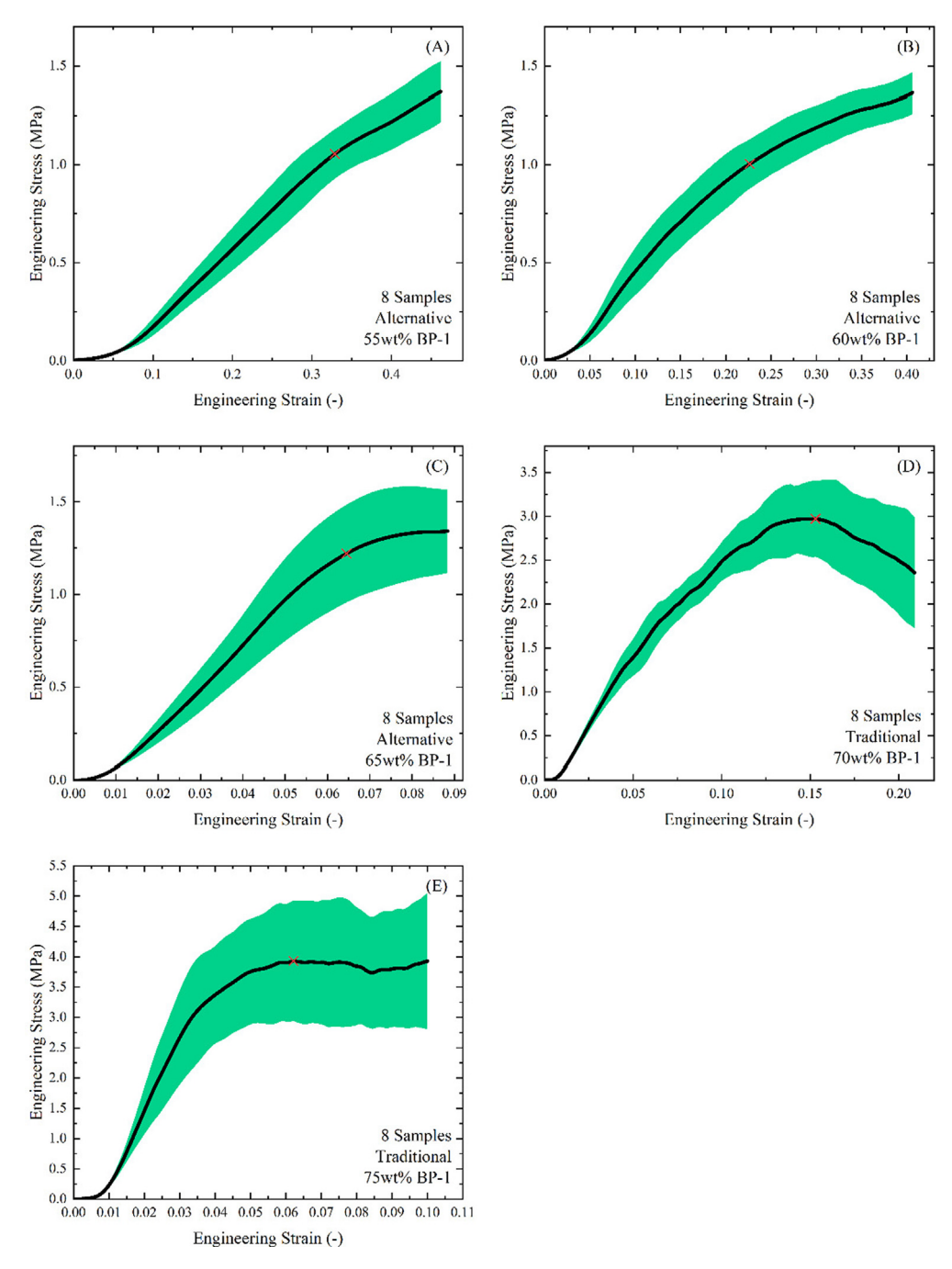


Fig. A7. Average engineering stress vs. engineering strain curves of BP-1 geopolymers, created from the  $0.5\text{Si}/\Sigma$  (60 H<sub>2</sub>O) activating solution, after 7 days of curing at ambient temperature and pressure. The green band represents  $\pm$  1 standard deviation and the red X indicates compressive strength and corresponding strain. The number of samples measured for each composition is indicated on the graph along with calculation method for compressive strength.

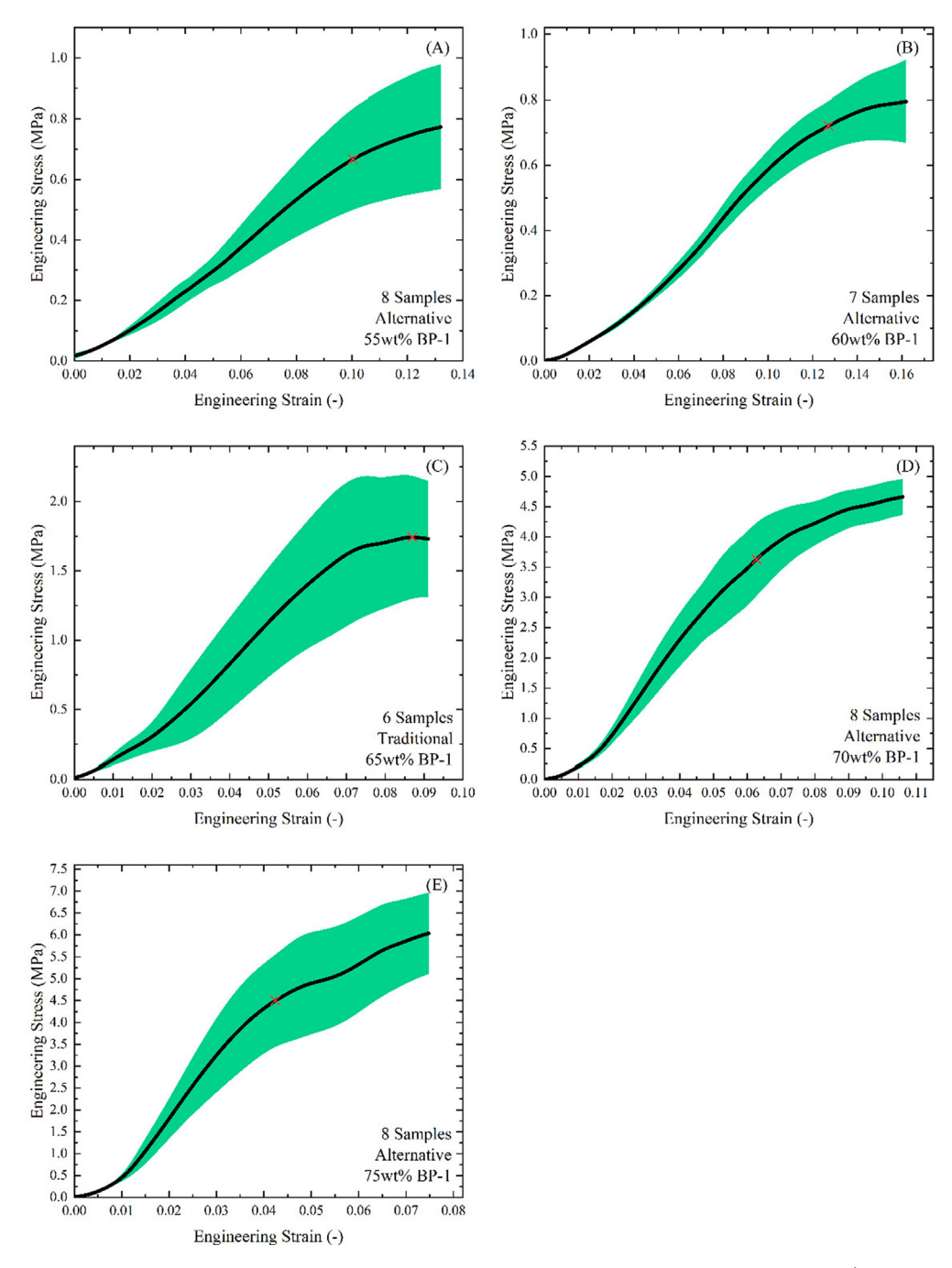


Fig. A8. Replicate average engineering stress vs. engineering strain curves of BP-1 geopolymers, created from the  $0.6\text{Si}/\Sigma$  (60  $\text{H}_2\text{O}$ ) activating solution, after 7 days of curing at ambient temperature and pressure. The green band represents  $\pm$  1 standard deviation and the red X indicates compressive strength and corresponding strain. The number of samples measured for each composition is indicated on the graph along with calculation method for compressive strength.

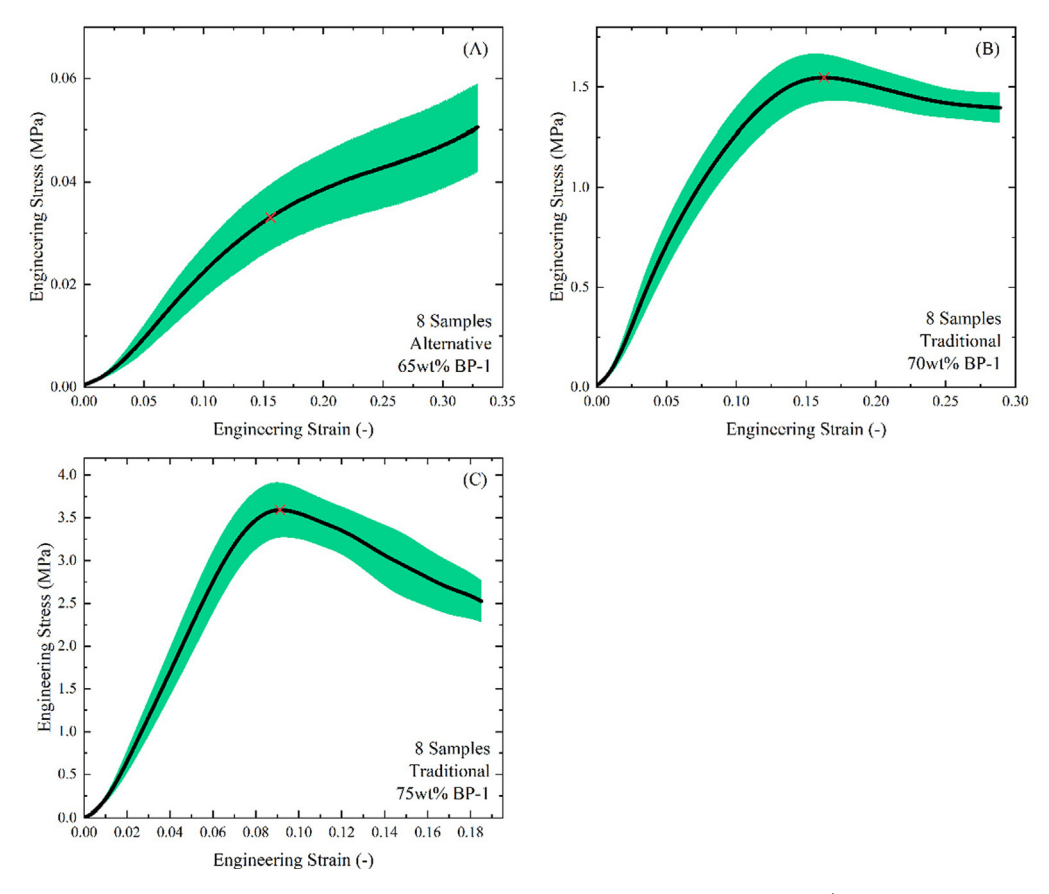


Fig. A9. Average engineering stress vs. engineering strain curves of BP-1 geopolymers, created from the  $0.4\text{Si}/\Sigma$  (45 H<sub>2</sub>O) activating solution, after 7 days of curing at ambient temperature and pressure. The green band represents  $\pm$  1 standard deviation and the red X indicates compressive strength and corresponding strain. The number of samples measured for each composition is indicated on the graph along with calculation method for compressive strength. Formulations with 55 wt% and 60 wt% BP-1 did not form a solid at seven-days.

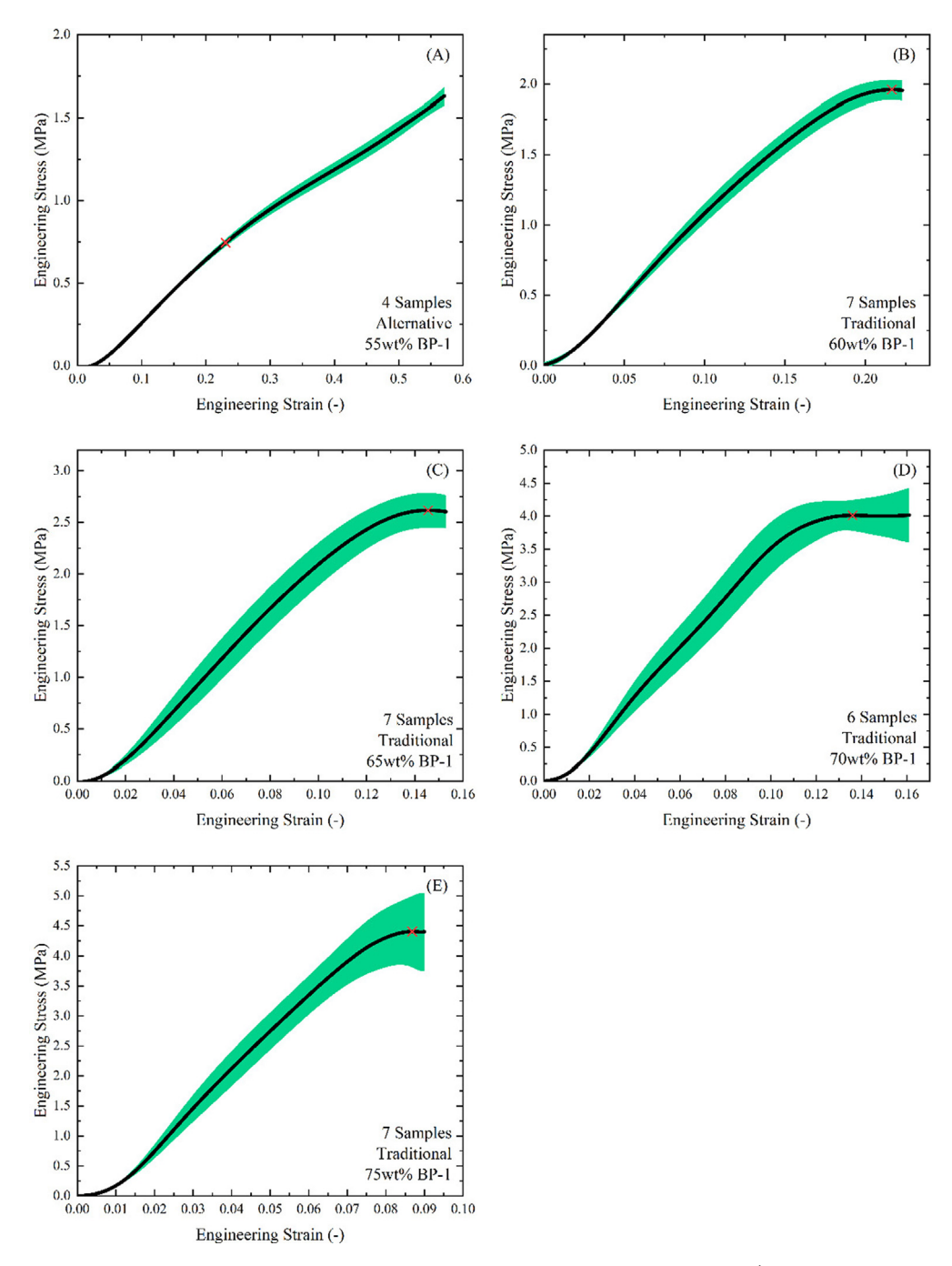


Fig. A10. Average engineering stress vs. engineering strain curves of BP-1 geopolymers, created from the  $0.5\text{Si}/\Sigma$  (45 H<sub>2</sub>O) activating solution, after 7 days of curing at ambient temperature and pressure. The green band represents  $\pm$  1 standard deviation and the red X indicates compressive strength and corresponding strain. The number of samples measured for each composition is indicated on the graph along with calculation method for compressive strength.

Table A1
Nomenclature appearing in the study listed in order of appearance.

Symbol / Abbreviation	Definition		
ISRU	In-situ Resource Utilization		
BP-1	Black Point-1 lunar regolith simulant		
Als	Aluminosilicates		
OPC	Ordinary Portland Cement		
JSC-1A	Johnson Space Center Lunar regolith simulant		
AM	Additive Manufacturing		
LHS-1	Lunar Highlands 1 regolith simulant		
MGS-1C	Mars Global Hydrated Clay Martian regolith simulant		
VTVL	Vertical Takeoff/Vertical Landing		
LOI	Loss on Ignition		
$\mathrm{Si}/\Sigma$	Molar ratio of Si to $(Si + Na)$ in activating solution		
CS	seven-day Compressive Strength		
MAS NMR	Magic Angle Spinning Nuclear Magnetic Resonance Spectroscopy		
E	Secant modulus		
$\sigma$	Engineering stress		
ε	Engineering strain		
F	Measured force		
$\Delta h$	Displacement		
h	Height of cube		
A	Contact surface area of cube		
$\sigma_2$	40 % of compressive strength		
$arepsilon_1$	Strain of 0.000050		
$arepsilon_2$	Corresponding strain to $\sigma_2$		
$\sigma_1$	Corresponding stress to $\varepsilon_1$		

Table A2
BP-1 geopolymer compositions created for this study on a per gram basis. Relevant nominal elemental ratios are also included for comparison to geopolymer materials from other aluminosilicate sources.

Activating Solution	Composition (wt% BP-1)	Mass BP-1	Mass SiO2	Mass NaOH	Mass H2O	Nominal Si/Al Ratio	Nominal Si/Na Ratio	Nominal Si/H2O Ratio
0.3Si/Σ (60 H <sub>2</sub> O)	55	0.55	0.07	0.11	0.27	3.07	1.64	0.37
,	60	0.60	0.06	0.10	0.24	2.95	1.85	0.43
	65	0.65	0.05	0.09	0.21	2.84	2.10	0.51
	70	0.70	0.05	0.07	0.18	2.76	2.41	0.63
	75	0.75	0.04	0.06	0.15	2.68	2.77	0.78
$0.4\text{Si}/\Sigma \ (60 \text{ H}_2\text{O})$	55	0.55	0.09	0.09	0.27	3.25	2.03	0.39
· · · · · · · · · · · · · · · · · · ·	60	0.60	0.08	0.08	0.24	3.10	2.26	0.45
	65	0.65	0.07	0.07	0.21	2.97	2.53	0.54
	70	0.70	0.06	0.06	0.18	2.85	2.85	0.65
	75	0.75	0.05	0.05	0.15	2.76	3.22	0.81
$0.5 \text{Si}/\Sigma (60 \text{ H}_2\text{O})$	55	0.55	0.11	0.07	0.27	3.42	2.53	0.41
. ( - /	60	0.60	0.10	0.06	0.24	3.23	2.78	0.47
	65	0.65	0.08	0.06	0.21	3.07	3.06	0.56
	70	0.70	0.07	0.05	0.18	2.94	3.37	0.67
	75	0.75	0.06	0.04	0.15	2.82	3.74	0.83
$0.6\text{Si}/\Sigma \ (60 \ \text{H}_2\text{O})$	55	0.55	0.12	0.06	0.27	3.57	3.20	0.43
	60	0.60	0.11	0.05	0.24	3.36	3.45	0.49
	65	0.65	0.10	0.04	0.21	3.18	3.72	0.57
	70	0.70	0.08	0.04	0.18	3.02	4.03	0.69
	75	0.75	0.07	0.03	0.15	2.89	4.38	0.84
$0.4\text{Si}/\Sigma \ (45 \text{ H}_2\text{O})$	55	0.55	0.12	0.12	0.20	3.57	1.72	0.57
	60	0.60	0.11	0.11	0.18	3.35	1.93	0.66
	65	0.65	0.10	0.10	0.16	3.18	2.14	0.77
	70	0.70	0.08	0.08	0.13	3.02	2.42	0.92
	75	0.75	0.07	0.07	0.11	2.89	2.74	1.12
$0.5 \text{Si}/\Sigma \text{ (45 H}_2\text{O)}$	55	0.55	0.15	0.10	0.20	3.80	2.20	0.60
	60	0.60	0.13	0.09	0.18	3.54	2.41	0.69
	65	0.65	0.12	0.08	0.16	3.32	2.65	0.80
	70	0.70	0.10	0.07	0.14	3.14	2.94	0.95
	75	0.75	0.08	0.05	0.11	2.98	3.28	1.16

Table A3

Material property results and water content information for BP-1 geopolymers after seven days of ambient curing.

<b>Activating Solution</b>	Composition (wt% BP-1)	Water Loss During 7-Day Ambient Curing (Mass frac.)	Compressive Strength (MPa)	Secant Modulus (MPa)	Strain to Fail (-)
0.3Si/Σ (60 H <sub>2</sub> O)	55	$0.24 \pm 0.01$	$0.19 \pm 0.06$	$4.74 \pm 1.79$	$0.04 \pm 0.01$
	60	$0.19 \pm 0.01$	$1.09 \pm 0.34$	$26.27 \pm 9.54$	$0.04 \pm 0.01$
	65	$0.2 \pm 0.02$	$2.39 \pm 0.85$	$44.93 \pm 13.41$	$0.09 \pm 0.01$
	70	$0.07 \pm 0.01$	$3.02 \pm 0.39$	$74.71 \pm 16.4$	$0.06 \pm 0.01$
	75	$0.25 \pm 0.03$	$5.3 \pm 1.12$	$147.34 \pm 37.66$	$0.06 \pm 0.02$
$0.4\text{Si}/\Sigma \ (60 \ \text{H}_2\text{O})$	55	$0.14 \pm 0$	$0.31 \pm 0.02$	$1.09 \pm 0.1$	$0.34 \pm 0.01$
	60	$0.11 \pm 0$	$0.53 \pm 0.04$	$2.01 \pm 0.22$	$0.25 \pm 0.01$
	65	$0.07 \pm 0.01$	$0.77 \pm 0.04$	$4.97 \pm 0.6$	$0.19 \pm 0.01$
	70	$0.07 \pm 0.01$	$1.3 \pm 0.14$	$13.55 \pm 2.18$	$0.12 \pm 0$
	75	$0.14 \pm 0.04$	$1.39 \pm 0.18$	$26.71 \pm 7.44$	$0.07 \pm 0$
0.5Si/Σ (60 H <sub>2</sub> O)	55	$0.21 \pm 0.01$	$0.78 \pm 0.09$	$5.02 \pm 1.09$	$0.22\pm0.02$
	60	$0.21 \pm 0.01$	$0.87 \pm 0.12$	$6.99 \pm 1.45$	$0.14 \pm 0.02$
	65	$0.18 \pm 0$	$1.41 \pm 0.25$	$20.17 \pm 4.07$	$0.06 \pm 0$
	70	$0.12 \pm 0.01$	$2.7 \pm 0.5$	$63.45 \pm 18.81$	$0.09 \pm 0.01$
	75	$0.18 \pm 0.02$	$4.61 \pm 0.98$	$112.75 \pm 25.15$	$0.05 \pm 0.01$
$0.6\text{Si}/\Sigma \ (60 \ \text{H}_2\text{O})$	55	N/A	$0.67 \pm 0.17$	$5.53 \pm 0.83$	$0.1 \pm 0$
	60	N/A	$0.72 \pm 0.07$	$4.69 \pm 0.39$	$0.13 \pm 0.01$
	65	N/A	$1.74 \pm 0.44$	$19.35 \pm 7.41$	$0.09 \pm 0$
	70	N/A	$3.63 \pm 0.6$	$49.93 \pm 9.5$	$0.06 \pm 0$
	75	N/A	$4.5 \pm 1.11$	$90.24 \pm 22.53$	$0.04 \pm 0$
$0.4 \text{Si}/\Sigma (45 \text{ H}_2\text{O})$	55	N/A	$0\pm0$	$0\pm0$	$0 \pm 0$
	60	N/A	$0\pm0$	$0\pm0$	$0 \pm 0$
	65	$0 \pm 0.02$	$0.03 \pm 0.01$	$0.2 \pm 0.05$	$0.16 \pm 0$
	70	$0 \pm 0.02$	$1.55 \pm 0.12$	$14.13 \pm 2.48$	$0.16 \pm 0.01$
	75	$0.07\pm0.04$	$3.59 \pm 0.32$	$41.05 \pm 6.41$	$0.09 \pm 0$
$0.5 \text{Si}/\Sigma \text{ (45 H}_2\text{O)}$	55	$0.14 \pm 0$	$0.74 \pm 0.07$	$2.7 \pm 0.14$	$0.23\pm0.01$
	60	$0.15 \pm 0.01$	$1.96 \pm 0.07$	$10.41 \pm 0.48$	$0.22 \pm 0$
	65	$0.14 \pm 0.03$	$2.62 \pm 0.17$	$19.16 \pm 3$	$0.15 \pm 0$
	70	$0.16 \pm 0.01$	$4.01 \pm 0.23$	$32.94 \pm 4.79$	$0.14 \pm 0.03$
	75	$0.13 \pm 0.04$	$4.4 \pm 0.59$	$51.14 \pm 7.47$	$0.09 \pm 0$

#### References

Al Bakri Abdullah, M. M., Kamarudin, H., Ismail, K. N., Bnhussain, M., Zarina, Y. & Rafiza, A. Correlation between Na2SiO3/NaOH ratio and fly ash/alkaline activator ratio to the strength of geopolymer. Advanced Materials Research, 2012. Trans Tech Publ, 189-193.

Al Bakri, A.M., Kamarudin, H., Bnhussain, M., Rafiza, A., Zarina, Y., 2012. Effect of Na^sub 2^SiO^sub 3^/NaOH Ratios and NaOH Molarities on Compressive Strength of Fly-Ash-Based Geopolymer. ACI Materials Journal 109, 503.

Alexiadis, A., Alberini, F., Meyer, M.E., 2017. Geopolymers from lunar and Martian soil simulants. Advances in Space Research 59, 490–495.

Anand, M., Crawford, I.A., Balat-Pichelin, M., Abanades, S., Van Westrenen, W., Péraudeau, G., Jaumann, R., Seboldt, W., 2012. A brief review of chemical and mineralogical resources on the Moon and likely initial in situ resource utilization (ISRU) applications. Planetary and Space Science 74, 42–48.

Astm International 2020. ASTM Standard C109. Standard Test Method for Compressive Strength of Hydraulic Cement Mortars (Using 2-in. or [50-mm] Cube Specimens).

Astm International 2022. ASTM C469. Standard Test Method for Static Modulus of Elasticity and Poisson's Ratio of Concrete in Compression. ASTM International.

Bakharev, T., 2005. Durability of geopolymer materials in sodium and magnesium sulfate solutions. Cement and Concrete Research 35, 1233–1246.

Barbosa, V.F.F., Mackenzie, K.J.D., Thaumaturgo, C., 2000. Synthesis and characterisation of materials based on inorganic polymers of

alumina and silica: sodium polysialate polymers. International Journal of Inorganic Materials 2, 309–317.

Chua, G. 2013. UQ's Global Change Institute first to use cement-free concrete for structural purposes. Available: https://www.geopolymer. org/news/70000-tonnes-geopolymer-concrete-airport/ [Accessed 3/15/2023].

Collins, P.J., Edmunson, J., Fiske, M., Radlińska, A., 2022. Materials characterization of various lunar regolith simulants for use in geopolymer lunar concrete. Advances in Space Research 69, 3941–3951.

Crawford, I.A., 2015. Lunar resources: A review. Progress in Physical Geography 39, 137–167.

Creech, S., Guidi, J. & Elburn, D. Artemis: An overview of NASA's activities to return humans to the moon. 2022 IEEE Aerospace Conference (AERO), 2022. IEEE, 1-7.

Davidovits, J., 2020. Geopolymer Chemistry and Applications. Institut Geopolymere, Saint-Quentin, France.

Davis, G., Montes, C., Eklund, S., 2017. Preparation of lunar regolith based geopolymer cement under heat and vacuum. Advances in Space Research 59, 1872–1885.

Doucet, F.J., Schneider, C., Bones, S.J., Kretchmer, A., Moss, I., Tekely, P., Exley, C., 2001. The formation of hydroxyaluminosilicates of geochemical and biological significance. Geochimica Et Cosmochimica Acta 65, 2461–2467.

Duxson, P., Provis, J.L., Lukey, G.C., Mallicoat, S.W., Kriven, W.M., Van Deventer, J.S.J., 2005a. Understanding the relationship between geopolymer composition, microstructure and mechanical properties. Colloids and Surfaces a: Physicochemical and Engineering Aspects 269, 47–58.

- Duxson, P., Provis, J.L., Lukey, G.C., Separovic, F., Van Deventer, J.S., 2005b. 29Si NMR study of structural ordering in aluminosilicate geopolymer gels, Langmuir 21, 3028–3036.
- Duxson, P., Fernández-Jiménez, A., Provis, J.L., Lukey, G.C., Palomo, A., Van Deventer, J.S.J., 2006. Geopolymer technology: the current state of the art. Journal of Materials Science 42, 2917–2933.
- Duxson, P., Mallicoat, S.W., Lukey, G.C., Kriven, W.M., Van Deventer, J.S.J., 2007a. The effect of alkali and Si/Al ratio on the development of mechanical properties of metakaolin-based geopolymers. Colloids and Surfaces a: Physicochemical and Engineering Aspects 292, 8–20.
- Duxson, P., Provis, J.L., Lukey, G.C., Van Deventer, J.S.J., 2007b. The role of inorganic polymer technology in the development of 'green concrete'. Cement and Concrete Research 37, 1590–1597.
- Engelhardt, G., Michel, D., 1987. High-resolution solid-state NMR of silicates and zeolites. Wiley, Chichester, U.K.
- Fernández-Jimenez, A., De La Torre, A., Palomo, A., López-Olmo, G., Alonso, M., Aranda, M., 2006. Quantitative determination of phases in the alkali activation of fly ash. Part i. Potential Ash Reactivity. Fuel 85, 625–634.
- Fernández-Jiménez, A., Palomo, A., Sobrados, I., Sanz, J., 2006. The role played by the reactive alumina content in the alkaline activation of fly ashes. Microporous and Mesoporous Materials 91, 111–119.
- Giuli, G., Bonazzi, P., Menchetti, S., 1999. Al-Fe disorder in synthetic epidotes: A single-crystal X-ray diffraction study. American Mineralogist 84, 933–936.
- Glasby, T., Day, J., Genrich, R., Aldred, J., 2015. EFC geopolymer concrete aircraft pavements at Brisbane West Wellcamp Airport. Concrete 2015, 1–9.
- Hardjito, D., Wallah, S.E., Sumajouw, D.M., Rangan, B.V., 2004a. Factors influencing the compressive strength of fly ash-based geopolymer concrete. Civil Engineering Dimension 6, 88–93.
- Hardjito, D., Wallah, S.E., Sumajouw, D.M., Rangan, B.V., 2004b. On the development of fly ash-based geopolymer concrete. Materials Journal 101, 467–472.
- He, P., Wang, M., Fu, S., Jia, D., Yan, S., Yuan, J., Xu, J., Wang, P., Zhou, Y., 2016. Effects of Si/Al ratio on the structure and properties of metakaolin based geopolymer. Ceramics International 42, 14416– 14422.
- Frazier, S. 2022. NASA, ICON Advance Lunar Construction Technology for Moon Missions. In: Bardan, R. (Ed.). NASA.gov.Website: https://www.nasa.gov/centers-and-facilities/marshall/nasa-icon-advance-lunar-construction-technology-for-moon-missions/
- Heiney, A. 2020. Regolith Resources. Available: https://www.nasa.gov/ offices/education/centers/kennedy/technology/nasarmc/RulesRubrics-Resources [Accessed May 26, 2023].
- Hewlett, P., Liska, M., 2019. Lea's chemistry of cement and concrete. Butterworth-Heinemann, Oxford, U.K.
- Hos, J., Mccormick, P., Byrne, L., 2002. Investigation of a synthetic aluminosilicate inorganic polymer. Journal of Materials Science 37, 2311–2316.
- Houston, J., Herberg, J., Maxwell, R., Carroll, S., 2008. Association of dissolved aluminum with silica: Connecting molecular structure to surface reactivity using NMR. Geochimica Et Cosmochimica Acta 72, 3326–3337.
- Jamkar, S., Ghugal, Y., Patankar, S., 2013. Effect of fly ash fineness on workability and compressive strength of geopolymer concrete. The Indian Concrete Journal 87, 57–61.
- Jones, H. The recent large reduction in space launch cost. 2018. 48th International Conference on Environmental Systems.
- Kaze, R., A Moungam, L. B., Djouka, M. F., Nana, A., Kamseu, E., Melo, U. C. & Leonelli, C. 2017. The corrosion of kaolinite by iron minerals and the effects on geopolymerization. Applied Clay Science, 138, 48-62.
- Kim, E. 2012. Understanding effects of silicon/aluminum ratio and calcium hydroxide on chemical composition, nanostructure and compressive strength for metakaolin geopolymers.

- Lee, S.K., Stebbins, J.F., 1999. The degree of aluminum avoidance in aluminosilicate glasses. American Mineralogist 84, 937–945.
- Löwenstein, W., 1954. The distribution of aluminum in the tetrahedra of silicates and aluminates. American Mineralogist: Journal of Earth and Planetary Materials 39, 92–96.
- Mao, Q., Li, Y., Liu, K., Peng, H., Shi, X., 2022. Mechanism, characterization and factors of reaction between basalt and alkali: Exploratory investigation for potential application in geopolymer concrete. Cement and Concrete Composites 130, 104526.
- Mckay, D.S., Heiken, G., Basu, A., Blanford, G., Simon, S., Reedy, R., French, B.M., Papike, J., 1991. The Lunar Regolith. *Lunar Sourcebook* 567, 285–356.
- Mckay, D.S., Carter, J.L., Boles, W.W., Allen, C.C., Allton, J.H., 1993.
  JSC-1: A new lunar regolith simulant. Lunar and Planetary Science Conference.
- Mills, J.N., Katzarova, M., Wagner, N.J., 2022b. Comparison of lunar and Martian regolith simulant-based geopolymer cements formed by alkali-activation for in-situ resource utilization. Advances in Space Research 69, 761–777.
- Mills, J., Mondal, P., Wagner, N., 2022a. Structure-property relationships and state behavior of alkali-activated aluminosilicate gels. Cement and Concrete Research 151, 106618.
- Mindess, S., 2019. Developments in the Formulation and Reinforcement of Concrete. Woodhead Publishing.
- Montes, C., Broussard, K., Gongre, M., Simicevic, N., Mejia, J., Tham, J., Allouche, E., Davis, G., 2015. Evaluation of lunar regolith geopolymer binder as a radioactive shielding material for space exploration applications. Advances in Space Research 56, 1212–1221.
- Nongnuang, T., Jitsangiam, P., Rattanasak, U., Tangchirapat, W., Suwan, T., Thongmunee, S., 2021. Characteristics of waste iron powder as a fine filler in a high-calcium fly ash geopolymer. Materials 14, 2515.
- Palomo, A., Blanco-Varela, M.T., Granizo, M., Puertas, F., Vazquez, T., Grutzeck, M., 1999. Chemical stability of cementitious materials based on metakaolin. Cement and Concrete Research 29, 997–1004.
- Palomo, A., Alonso, S., Fernandez-Jiménez, A., Sobrados, I., Sanz, J., 2004. Alkaline activation of fly ashes: NMR study of the reaction products. Journal of the American Ceramic Society 87, 1141–1145.
- Papike, J., Simon, S., Laul, J., 1982. The lunar regolith: Chemistry, mineralogy, and petrology. Reviews of Geophysics 20, 761–826.
- Pilehvar, S., Arnhof, M., Pamies, R., Valentini, L., Kjøniksen, A.-L., 2020. Utilization of urea as an accessible superplasticizer on the moon for lunar geopolymer mixtures. Journal of Cleaner Production 247.
- Pouhet, R., Cyr, M., Bucher, R., 2019. Influence of the initial water content in flash calcined metakaolin-based geopolymer. Construction and Building Materials 201, 421–429.
- Provis, J.L., Duxson, P., Lukey, G.C., Separovic, F., Kriven, W.M., Van Deventer, J.S., 2005. Modeling speciation in highly concentrated alkaline silicate solutions. Industrial & Engineering Chemistry Research 44, 8899–8908.
- Provis, J., Van Deventer, J., 2007. Geopolymerisation kinetics. 2. Reaction Kinetic Modelling. Chemical Engineering Science 62, 2318–2329
- Rahmatian, L. A. & Metzger, P. T. 2010. Soil test apparatus for lunar surfaces. Earth and Space 2010: Engineering, Science, Construction, and Operations in Challenging Environments.
- Ray, C., Reis, S., Sen, S., O'dell, J., 2010. JSC-1A lunar soil simulant: Characterization, glass formation, and selected glass properties. Journal of Non-Crystalline Solids 356, 2369–2374.
- Rees, C.A., Provis, J.L., Lukey, G.C., Van Deventer, J.S., 2007. Attenuated total reflectance fourier transform infrared analysis of fly ash geopolymer gel aging. Langmuir 23, 8170–8179.
- Rickard, W.D., Riessen, A.V., Walls, P., 2010. Thermal character of geopolymers synthesized from class F fly ash containing high concentrations of iron and α-quartz. International Journal of Applied Ceramic Technology 7, 81–88.

- Roussel, N., 2018. Rheological requirements for printable concretes. Cement and Concrete Research 2018, 76-85
- Rovnaník, P., 2010. Effect of curing temperature on the development of hard structure of metakaolin-based geopolymer. Construction and Building Materials 24, 1176–1183.
- Sagoe-Crentsil, K., Weng, L., 2006. Dissolution processes, hydrolysis and condensation reactions during geopolymer synthesis: Part II. High Si/Al ratio systems. Journal of Materials Science 42, 3007–3014.
- Sanders, G.B., Larson, W.E., 2012. Progress made in lunar in situ resource utilization under NASA's exploration technology and development program. Earth and Space 2012: Engineering, Science, Construction, and Operations in Challenging Environments, 457–478.
- Saraya, M.-E.-S.-I., El-Fadaly, E., 2017. Preliminary study of alkali activation of basalt: effect of NaOH concentration on geopolymerization of basalt. Journal of Materials Science and Chemical Engineering 5, 58–76.
- Shi, H., Ma, H., Tian, L., Yang, J., Yuan, J., 2020. Effect of microwave curing on metakaolin-quartz-based geopolymer bricks. Construction and Building Materials 258.
- Silva, P.D., Sagoe-Crenstil, K., Sirivivatnanon, V., 2007. Kinetics of geopolymerization: Role of Al2O3 and SiO2. Cement and Concrete Research 37, 512–518.
- Smith, M., Craig, D., Herrmann, N., Mahoney, E., Krezel, J., Mcintyre, N., Goodliff, K., 2020. The Artemis Program: An Overview of NASA's Activities to Return Humans to the Moon. IEEE.
- Stoeser, D., Wilson, S. A. & Rickman, D. L. 2010. Preliminary geological findings on the BP-1 simulant. National Aeronautics and Space Administration, Marshall Space Flight Center.
- Suescun-Florez, E., Roslyakov, S., Iskander, M., Baamer, M., 2015. Geotechnical Properties of BP-1 Lunar Regolith Simulant. Journal of Aerospace Engineering 28, 04014124.

- Valcke, S.L., Pipilikaki, P., Fischer, H.R., Verkuijlen, M.H., Van Eck, E. R., 2015. FT-IR and 29 Si-NMR for evaluating aluminium-silicate precursors for geopolymers. Materials and Structures 48, 557–569.
- Vitola, L., Pundiene, I., Pranckeviciene, J., Bajare, D., 2020. The impact of the amount of water used in activation solution and the initial temperature of paste on the rheological behaviour and structural evolution of metakaolin-based geopolymer pastes. Sustainability 12, 8716
- Wang, K.-T., Lemougna, P.N., Tang, Q., Li, W., Cui, X.-M., 2017. Lunar regolith can allow the synthesis of cement materials with near-zero water consumption. Gondwana Research 44, 1–6.
- Warner, C. M. 2020. Lunar Living: NASA's Artemis Base Camp Concept. Available from: https://blogs.nasa.gov/artemis/2020/10/28/lunar-living-nasas-artemis-base-camp-concept/ [Accessed October 28, 2020 2023].
- Weng, L., Sagoe-Crentsil, K., 2007. Dissolution processes, hydrolysis and condensation reactions during geopolymer synthesis: Part I—Low Si/ Al ratio systems. Journal of Materials Science 42, 2997–3006.
- Williams, J.-P., Paige, D., Greenhagen, B., Sefton-Nash, E., 2017. The global surface temperatures of the Moon as measured by the Diviner Lunar Radiometer Experiment. Icarus 283, 300–325.
- Xie, J., Kayali, O., 2014. Effect of initial water content and curing moisture conditions on the development of fly ash-based geopolymers in heat and ambient temperature. Construction and Building Materials 67, 20–28.
- Zhou, S., Lu, C., Zhu, X., Li, F., 2020. Preparation and characterization of high-strength geopolymer based on BH-1 lunar soil simulant with low alkali content. Engineering 7, 1631–1645.
- Zuhua, Z., Xiao, Y., Huajun, Z., Yue, C., 2009. Role of water in the synthesis of calcined kaolin-based geopolymer. Applied Clay Science 43, 218–223.